AMERICAN UNIVERSITY OF BEIRUT

EXPERIMENTS ON THE HEATING AND MECHANICAL EFFECTS OF HIGH INTENSITY FOCUSED ULTRASOUND

by
MOATH MUSTAFA QURAINI

A thesis
submitted in partial fulfillment of the requirements
for the degree of Master of Engineering
to the Department of Mechanical Engineering
of the Faculty of Engineering and Architecture
at the American University of Beirut

Beirut, Lebanon
September 2012

AMERICAN UNIVERSITY OF BEIRUT

EXPERIMENTS ON THE HEATING AND MECHANICAL EFFECTS OF HIGH INTENSITY FOCUSED ULTRASOUND

by

MOATH MUSTAFA QURAINI

Approved by:

Dr. Ghanem F. Oweis, Assistant Professor Department of Mechanical Engineering	Advisor
Dr. Alan L. Shihadeh, Associate Professor Department of Mechanical Engineering	Member of Committee
Dr. Ghassan Antar, Associate Professor Department of Physics	Member of Committee

Date of thesis defense: September 20, 2012

AMERICAN UNIVERSITY OF BEIRUT

THESIS RELEASE FORM

I, Moath Mustafa Quraini

☐ authorize the American University of Beirut to supply copies of my thesis to libraries or individuals upon request.

☐ do not authorize the American University of Beirut to supply copies of my thesis/dissertation/project to libraries or individuals for a period of two years starting with the date of the thesis defense.

_____
Signature

_____
Date

ACKNOWLEDGMENTS

This thesis would have not been possible unless with the support, guidance, and encouragement of my advisor, Prof. Ghanem Oweis. I want to heartily thank him for his time and effort working proximally to polish this work. I would also like to thank Prof. Michael Baily at Center of Industrial and Medical Ultrasound (CIMU) at University of Washington for motivating this work, and special thanks to Prof. Michael Canney at Inserm, LabTau at Université de Lyon, for his valuable input to make this project available at its best shape.

I would also like to thank my beloved parents and family, for their care and support. Lastly, I would like to thank the committee of my thesis Prof. Alan Shihadeh , and Prof. Ghassan Antar for their time and effort and criticism in making my thesis better presented.

AN ABSTRACT OF THE THESIS OF

Moath Mustafa Quraini for Master of Engineering
Major: Mechanical Engineering

Title: Experiments on the Heating and Mechanical Effects of High Intensity Focused Ultrasound

Free field experimental measurements of the temperature rise of water and tissue deformation in the focal region of a 2 MHz high intensity focused ultrasound (HIFU) transducer were performed. Millisecond pulsed HIFU was operated at acoustic focal intensities in the range of 1,200 W/cm2 and up to 18,500 W/cm2, resulting in nonlinear wave propagation and shock wave formation. Pulsed, planar laser-induced fluorescence (LIF) was used as a fast-rise-time, non-intrusive, temperature measurement method of the water present in the focal region. The laser light sheet was oriented transverse to the acoustic axis. Cross-sectional, instantaneous temperature field measurements within the HIFU focal volume revealed that the water temperature increased steadily with increasing the HIFU input power. We measured heating rates of 4000-7000 ^{0}C /sec within the first millisecond of the HIFU burst. Increasing the length of the burst initially resulted in an increase in the water temperature within the HIFU focal spot (up to 2.5 ms), after which it steadied or slightly dropped. Acoustic streaming was measured and shown to be consistent with the reduction in heating with increased burst length due to the convective cooling effect. Furthermore, the deformation and mechanical effects on tissue due to pulse HIFU is studied. Deformation field were measured using Laser Digital Image Correlation technique. Compressive deformation mechanisms in the micron scale were observed at the focal point.

CONTENTS

ACKNOWLEDGEMENTS..... v

ABSTRACT..... vi

LIST OF ILLUSTRATIONS..... ix

LIST OF TABLES..... xii

Chapter

1. INTRODUCTION..... 1

1.1. Background:..... *2*

1.1.1. Piezoelectricity & Transducers:..... 2
1.1.2. Ultrasound Wave Propagation & Non-Linear Effects:..... 4
1.1.3. Acoustic Streaming:..... 6
1.1.4. Acoustic Cavitation:..... 6
1.1.5. Heating and Shock Induced Heating: 8

1.2. Literature Review: *8*

1.3. Objectives: *12*

2. METHODS AND EXPERIMENTAL SETUP 14

2.1.Laser Induced Fluorescence Thermometry of Pulsed HIFU*:*..... *14*

2.1.1. HIFU Transducer..... 16
2.1.2. Water Bath..... 16
2.1.3. Laser Induced Fluorescence LIF..... 17

2.2. Particle Image Velocimetry of Pulsed HIFU in Water*:*..... *21*

2.3. Pulsed HIFU Laser Digital Image Correlation and High speed imaging in Clear Tissue Mimicking Phantom:…….…..…….. 23

2.4. Calibration of HIFU Transducer Using Radiation Force Balance:..... *25*

3. RESULTS 28

3.1. Laser Induced Fluorescence Temperature Measurement *28*

3.2. Acoustic Field Velocity Measurements in Water *40*

3.3.Tissue Mimicking Phantom Rapture and Deformation Experiments:..... *42*

3.4. High Intensity Focused Ultrasound Transducer Calibration *50*

4. DISCUSSION 53

5. CONCLUSION 63

REFERENCES 64

ILLUSTRATIONS

Figure Page

1. A schematic of the Direct Piezoelectric Effect. 2
2. A schematic of the Converse Piezoelectric Effect 3
3. Spherically Focused Ultrasound Transducer..... 4
4. Measurement of a 2 khz sound wave propagated through a plastic tube at enternece and after three meters of propagation 4
5. (a) Schematic of the LIF setup (The same schematic works with the PIV and LDIC). (b) Image of the LIF setup and the fluorescence vail. (c) LIF timing schematic..... 15
6. Sample calibration curve of water averaged over 225×85 pixels 20
7. Radiation Force Balance calibration setup schematic..... 26
8. Images of the Radiation Force Balance Calibration setup 26
9. (a) Longitudinal cut through HIFU focal spot shows spherical focusing waves that matches the 0.69 mm wavelength - 10 ms pulse at 14,000 W/cm^2 the cut was taken 9ms within the 10 ms burts. (b) Longitudinal cut through HIFU focal spot shows shadowing artifact after a 10 ms pulse at 14,000 W/cm^2 29
10. (a) Rhodamine B temperature dependent intensity dye sonicated showing the dye intensity decreasing at the focal point due to the temperature increase at the focal spot along with the shadowing artifact. (b) Rhodamine 6G temperature independent day show 31
11. (a) Heated sport temperature distribution , with Gaussian profile (b) numerical model of the heated spot shows shadowing artifact. 33
12. Cuts through the heated spot show non-calibrated intensity images to show the shape of the heated spot. 34
13. Temeprature field deteremined by LIF experiments of the cross section of the HIFU in water and 20% gly. solution with RhB at 14,000W/cm^2 (a,b,c, and d are in water, while e,f,g, and h are in 20% Gly. solution)..... 35
14. Temperature profile though radial cuts for different sonication exposures. 37
15. (a) Temperature rise vs. number of cycles in two bursting methods in water-RhB solution. (b) Temperature rise vs. Number of cycles for (Water and 20% Gly. - RhB Solutions at 14,000 W/cm2) 38
16. (a) Temperature rise vs. number of cycles for operating focal intensities of 14,000 and 18,500 W/cm2. (b) Temperature rise vs. operating peak to peak voltage for two number HIFU exposure (3-10 ms)..... 39

17. (a) vector field of a 3ms HIFU burst delayed by 0.5 ms after burst at 14,000 W/cm^2 focal intensity. (b) cut through the vector field as indicated in fig.17 (a). 41
18. Top illuminated RTV-615 tissue mimicking material exposed to pulsed HIFU at 18,300 W/cm^2 using PCO integrated image frame mode..... 42
19. Scatter plot of tear length vs. focal intensity of pulsed HIFU at exposures between 4316 and 10790 cycles. 43
20. Phantom High speed camera imaging showing the initiation and growth of the tear in RTV 615 at 5 ms exposure with HIFU operating at 18,300 W/cm^2 captured at 13,029 fps 44
21. (a) axial section of LDIC displacement vector field take at focal intensity of 5,200 W/cm^2 with pulse duration of 1 ms. (b) cross-sectional LDIC displacement field taken at 2,500 W/cm^2 and HIFU pulse duration fo1 ms. 46
22. $\boldsymbol{D_{total}}$ of an axial displacement field from LDIC in RTV-615 by pulsed HIFU operated at 5,200 W/cm^2 at the end of a 1 msec pulse. 47
23. $\boldsymbol{D_{total}}$ of a cross-section displacement field from LDIC in RTV-615 by pulsed HIFU operated at 2,500 W/cm2 at the end of a 1 msec pulse. 48
24. Cuts through cross-sectinal displacement field determined by LDIC of RTV-615 from pulsed HIFU operated at different focal intensities at 1079 cycles (0.5 msec) 48
25. *dV/dy* Strain field determined using least square method using deformation field aquired by LDIC experiment of pulsed HIFU operated at focal intensity of 5,200 W/cm^2 and pulse duration of 4316 cycles..... 49
26. Axial stress field of a pulsed HIFU at focal intensity of 5,200 W/cm^2 and a pulse duration of 1 msec..... 50
27. Radiation force balance setup force on acoustic absorber. 51
28. Radiation force balance experiment calibration curve of the acoustic power vs. the peak to peak voltage input to the transducer with and without saran wrap to avoid streaming 51
29. The Fundamental peak to peak voltage vs. The focal intensity of the HIFU transducer determined by the RFB setup 52
30. (a) Acoustic particle velocity waveform in the HIFU focal region measured with PIV. The two PIV image exposures are taken 250 ns apart at the end of a 15-cycle burst. Each curve is averaged from 40 instantaneous vector fields. (b) the 1200 W/cm2 focal intensity; and (c), the 18,500 W/cm2 focal intensity. The US propagation is from right to left. 55
31. (a) total acoustic particle velocity field in the HIFU focal region measured with PIV at the end of a 15-cycle burst at different focal intensities showing the narrowing of the waves that caused the phase shift in the cuts. 56

Dedication addressed

To my family

CHAPTER 1

INTRODUCTION

Research efforts into the physics and mechanics of high intensity focused ultrasound (HIFU) devices have expanded over the last decade due to a renewed interest in their medical relevance as a surgical and a therapeutic tool since their initial introduction in the 1940's and 50's. Efforts have focused on two aims; to provide an improved understanding of the HIFU outcomes upon interaction between the propagating sound and its surrounding medium be it tissue or otherwise; and to develop dependable characterization and metrological tools that could be used to robustly quantify and predict the energetic and temperature outputs of HIFU transducers originating from different manufacturers particularly when used in a clinical setting (Curra & Crum 2003; Harris 2003; ter Haar 2007; Shaw & Hodnett 2008). The challenge in understanding the output from HIFUs stems from the fact that clinical devices can operate at peak focal intensities of 1,000 to more than 10,000 W/cm^2. Typically, a HIFU source is first characterized in water, the spatial field is characterized at low intensity levels, where acoustic propagation is linear, and then the results are derated to predict the field in tissue. The challenges in performing this process are illustrated in the recent work of Canney et al. (2008). The major effects of HIFU upon interaction with propagation medium are thoroughly discussed in the background section.

1.1. Background*:*

1.1.1. Piezoelectricity & Transducers:

Therapeutic ultrasound transducers are made out of piezoelectric crystals and in order to understand their behavior it is very important to understand the properties of piezoelectricity. An ultrasound transducer is a transducer that can convert the mechanical vibration into an electric current and vice versa (Rossing, 2007). Piezoelectric crystals such as PZT hold a property in which when an electrical current is applied on their surface the crystals would deform, and as the electrical current polarity is set to opposite the direction of the deformation would reverse such as from tension to compression. This effect is called the direct piezoelectric effect. **Fig.1** shows a schematic of the direct piezoelectric effect.

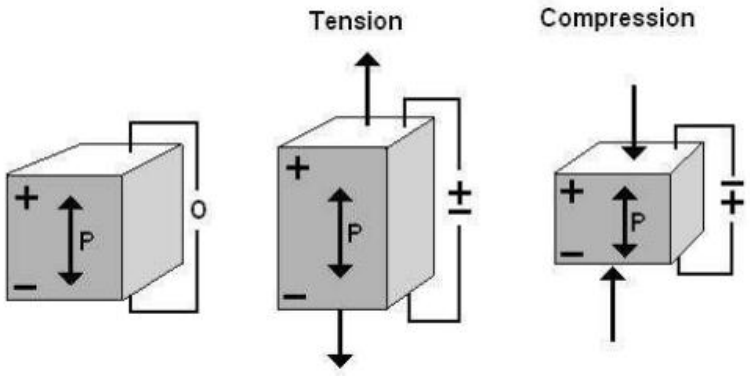

Fig. 1: A schematic of the Direct Piezoelectric Effect.

Moreover, piezoelectric crystals have the property of converting the mechanical strain into an electric field, and as the direction of the mechanical strain changes to opposite the polarity of the electrical current would change to opposite. This is called the converse piezoelectric effect. **Fig.2** shows a schematic of the converse piezoelectric effect.

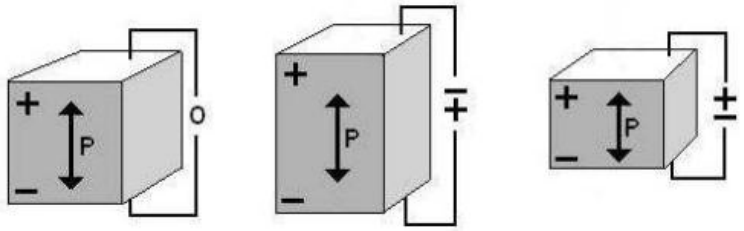

Fig. 2: A schematic of the Converse Piezoelectric Effect

When the piezoelectric crystals are subject to an AC current, the crystals would vibrate on the AC frequency on the AC current. However, for each piezoelectric crystal a fundamental resonance frequency exists such that at that frequency the amplitude of the vibration would be maximal. This frequency depends on the thickness of the piezoelectric crystal that is made. The thickness of the piezoelectric crystals represents half of the wave length. However, there are other frequencies that the crystals would respond to with high amplitudes, never the less the amplitude will not be higher than the fundamental resonance frequencies amplitudes. These frequencies are called higher harmonics, and they are formulated such that they are odd multiples of half of the wavelength (Vives, 2008).

In therapeutic ultrasound, the properties of piezoelectricity are used to vibrate the piezoelectric crystals at their resonance frequency. This resonance at high frequencies would emit ultrasound. High Intensity Focused Ultrasound (HIFU) is achieved by geometrically focusing the ultrasound waves emitted from the transducer into a focal point such as spherically focused ultrasound transducers. **Fig.3** shows a schematic of a spherically focused ultrasound transducer.

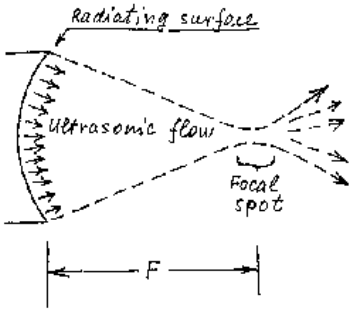

Fig. 3: Spherically Focused Ultrasound Transducer

1.1.2. Ultrasound Wave Propagation & Non-Linear Effects:

Nonlinear physical phenomena were first observed in the field of acoustics. Propagation of sound at low intensities for small distances in mostly considered to be linear propagation, however as the distance increases the nonlinear effects starts to be more distinct. **Fig.4** shows the steepening and change of form of a sound wave propagating at 2 kHz guided inside a plastic tube filled with air. The sound wave was measured at the inlet of the tube and after three meters of propagation.

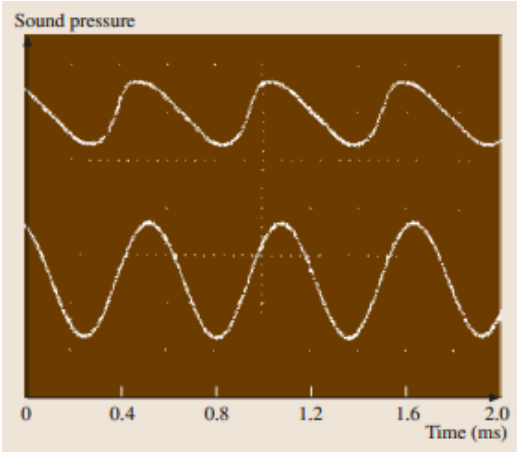

Fig. 4: Measurement of a 2 khz sound wave propagated through a plastic tube at enternece and after three meters of propagation

For short distance propagation nonlinear effects are always seen at high intensities. Some of the nonlinear effects are due to the nonlinearities in the medium of propagation. For a single harmonic wave with a frequency f propagating through a medium with nonlinearities, higher harmonics are generated at high intensities such that, $f_m = m f$. Higher harmonics cause steeping of the wave and can lead to formation of shockwaves.

Some other nonlinear effects are generated by self-action by the high intensity waves. The self-action is primary due to the change of the properties of the medium of propagation by the sound wave itself. There are several nonlinear effects that are associated with high intensities such as transmitting force to the medium of propagation setting the medium into motion (acoustic streaming). One of the nonlinear phenomena that cause a wide variety of effects related to it is the rapture of the liquid medium by the propagating sound waves which is called acoustic cavitation. Acoustic cavitation is a trigger for special effects that are related to the bubble dynamics in the liquid mediums. Some of these effects are the collapse of the bubble which causes sonoluminescence, and or chemical reaction (sonochemistry). Thermal effect due the non-linear wave propagation through mediums in the case of HIFU is very important due to its therapeutic applications (Rossing, 2007).

In the following section the major nonlinear effects which are acoustic streaming, cavitation, heating and shock induced heating are going to be briefly described.

1.1.3. Acoustic Streaming:

The propagation of sound is known to generate motion into the fluidic medium. This motion is mostly due to the action of Reynolds's stress in the medium. The spatial gradient in the acoustic momentum flux due to the medium attenuation forces lead the acoustic streaming motions. The wave Reynolds stress is defined as ($\overline{\rho u_i u_j}$), the Reynolds stress spatial variation causes a force acting per unit volume is represented by $F_j = -\partial(\overline{\rho u_i u_j})/\partial x_j$.

Another source to the acoustic streaming is the unbalanced stresses that are caused by the attenuation. One of the theories that can further describe the acoustic streaming is the flow noise theory. The flow noise theory describes that the Reynolds stress is the mean value of the momentum fluid flux whose fluctuations in a flow field would generate flow noise (Lighhil, 1978).

1.1.4. Acoustic Cavitation:

It is hard to briefly define cavitation. A general way of defining cavitation is when a new surface is introduced in a liquid medium. A more broad definition would include the cavities introduced from the phenomena of boiling (Neppirans, 1980).

When an ultrasound wave is propagating through a liquid medium, it consists of a sinusoidal wave where it will increase the pressure of the liquid medium above the ambient pressure, at the refractive phase the pressure will drop to negative values. The drop in pressure in the medium in the refractive phase causes the dissolved gasses to go out of solution; this action of the gasses going out of solution after irradiation of the ultrasound wave is called acoustic cavitation (Kyuichi, 2010).

Nucleation of the acoustic cavitation is a place of controversy, but mainly it can be explained by one of three mechanisms. The first mechanism of cavitation nucleation in crevices. The surface tension inside a crevice would lead to a low pressure inside the gas pocket in the concave crevice. The lower pressure makes the gas pocket stabilized against dissolution in the liquid. The second mechanism is for nucleation is the present of bubbles inside the liquid that are stabilized in the medium due to the impurities that are on the surface of the bubble which are surfactants. Without the presence of the surfactants the bubbles which are below $1\ \mu m$ would directly dissolve in the liquid if it was not saturated. The third mechanism of acoustic cavitation, is the fragmentation of active cavitation bubbles. Unstable shaped bubbles are fragmented into daughter bubbles that are also new nuclei for cavitation bubble. The instability in the bubble shapes are usually caused by asymmetric environment (Kyuichi, 2010).

Acoustic cavitation can have two types that can be easily distinguished with their violent and gentle behavior. The cavities that are from the stable type they exist for many cycles. These stable cavities are known to oscillate around their equilibrium size nonlinearly. The other type of cavities which are known for their violence are the transient cavities. These cavities are usually shorter than a cycle. Transient cavities expand to more than double of their equilibrium size and then shrink and collapse. The collapse of these bubbles usually is followed by effects that drew the attention of researchers to the transient bubble phenomena and the effects after their collapse namely are erosion, emulsification, molecular degradation, sonluminescence, sonochemistry, and biological effects (Neppirans, 1980).

1.1.5. Heating and Shock Induced Heating:

One of the most important effects that are important especially in the term of its therapeutic application is the heating effects of ultrasound. Ultrasound is known to be absorbed by its propagation medium depending on the mediums absorption and the frequency of the irradiated ultrasound beam. When the ultrasound source is going up to higher intensities, the nonlinear effects tend to increase. The nonlinearity tends to generate higher harmonics, which cause to higher absorption of the propagation medium to the ultrasound waves and a faster conversion of the acoustic energy into heat (Rossing, 2007).

In HIFU the acoustic energy levels are higher leading to more nonlinear effects during the propagation of sound. Mostly the upper part of the ultrasound wave is travelling faster than the lower side of the flow leading to accumulation of the waves and distortion of the temporal shape of the sound leading to the generation of the higher harmonics. The generation of higher harmonics leads at high intensities to formation of shockwaves. The shockwaves are reported to have significantly higher conversion of the acoustic energy to heat leading to shockwave boiling in therapeutic times which are in the order of seconds (Canney et al., 2008).

1.2. Literature Review*:*

Banerjee & Dasgupta (2010), provides a comprehensive review on the thermal characterization of HIFU. Computational-based thermal diagnostic is a prominent method in which the output acoustic field of HIFU is characterized accurately in water with a hydrophone, and then input to a numerical model combining the wave propagation and the heat diffusion equations to predict the temperature rise in tissue

(Khokhlova et al. 2006; Canney et al. 2008). Naturally, accurate physical properties need to be input to the model to provide clinically usable results, which may themselves be dependent on the degree of heating, and are not always straight forward to obtain. Acoustic streaming, measured using particle image velocimetry (PIV), has been used to characterize HIFU sources and to indirectly infer the heating output a posteriori. PIV is an optical imaging tool in which minute tracer particles are added to the flow and their visualization is made possible through the use of coherent light illumination. The flow velocities are measured by taking time-lapsed image pairs of the tracer particles, which are then mathematically correlated to infer the particle displacements. . Hariharan et al. (2008) used this technique and related the power output of a HIFU transducer to the steady streaming velocity for focal intensities O(1000 W/cm2). At these intensity levels, streaming velocities of several cm/s were measured.

A direct clinical temperature monitoring tool for HIFU therapy is magnetic resonance imaging MRI (Jolesz 2009; Dasgupta et al. 2010; Holbrook et al. 2010). Yet its bulky size, relative expense, and its spatial (~1 mm) and temporal resolutions (~1-5 seconds acquisition times) can significantly impair its use as a diagnostic laboratory tool (Khokhlova et al. 2009). With these limitations, focus on using diagnostic ultrasound US imaging to monitor heat treatments and assess clinical temperature rise from HIFU has significantly increased. A number of recent studies discuss the details of such implementations (Seip & Ebbini 1995; Qian et al. 2006; Speyer et al. 2010; Liu and Ebbini 2010). Still, clinical US imaging thermometry can be limited in spatial resolution, as well as in temporal resolution unless the so-called “ultrafast” scanners are used.

The use of thermocouples at the focal point in gels has been plentiful due to their low cost and simplicity of implementation, even when many have cautioned against their invasiveness and the significant temperature bias they can introduce through the viscous heating effect (Huang et al. 2004; Morris et al. 2008; Chen et al. 2009). Khokhlova et al. (2009), for example, measured temperatures of 100 ^{0}C in 0.5 seconds with a thermocouple present in a HIFU field, and 7 seconds without. A variation is to place an array of thermocouples off the acoustic beam axis and to use the data with a fitting function to extrapolate the temperature in the focal region. Thermocouples can also be limited in their temporal response (tens to hundreds of milliseconds) for the accurate resolution of shock heating.

Other studies report different HIFU thermometry methods including the use of infra-red thermal cameras, photoacoustic sensors, and liquid crystal sheets (Chitnis et al. 2009; Song et al. 2008; Shaw et al. 2011; Nishihara 2011), they vary in their range of applicability, accuracy, and noise levels. It can be noted that the majority of the HIFU temperature estimations listed above were done on tissue or tissue mimicking visco-elastic phantoms. Little work has targeted HIFU free-field heating in water possibly because of the general notion that the water absorption is very small and the typical propagation distance of interest is short to produce any noticeable losses especially when the wave propagation is linear. But the acoustic absorption in water is not exactly zero particularly when the wave propagation is non-linear as within the focus of high power HIFU and/or at high frequencies. Hall (1948) provides a molecular-based discussion on the source of acoustic absorption in water and how it relates to the medium compressibility. Yet the nearly lossless water path makes it all the more interesting in a laboratory setting to quantify localized HIFU heating in the presence of

non-linear and shock effects at the focus. Water studies have focused instead on the more tangible outcome of acoustic streaming (Hariharan et al. 2008). The one commonly used free field water temperature measurement from US exposure (Hallez et al. 2007) has been based on bulk fluid calorimetry, in which the overall deposited acoustic energy over relatively long insonification periods is quantified but not the local heating at the HIFU focus.

The effects of HIFU in tissue phantoms such as polyacrylamide and real tissue have been widely investigated (Canney et al. 2009; Canney el al. 2008; Khokhlova et al. 2011). Direct and violent effects that lead to instant damage to tissue are reported. Most of these effects are due to shock-induced heating and violent cavitation effects. Most of these effects are seen in high intensified ultrasound energy mode as discussed earlier. However, there have been plentiful evidence of other effects due to HIFU other than thermal and cavitation effects (Hancock el al. 2009; Nightingale 2001; Cheng et al. 2012), mechanical effects such as formation of ruptures and gaps have been suspected due to mechanical stresses in tissue. Opening of the Blood-Brain Barrier (BBB), using pulsed HIFU have been reported. This opening of BBB made drug delivery of chemotherapy possible (Hancock el al. 2009; Yang et al. 2012; Choi et al. 2006). However, a clear explanation of the mechanisms behind it and clear evidence is still vacant. In the study (HIFU gap formation), preliminary evidence of gap formation and raptures that are mechanically induced without presence of cavitation have been reported. However, not enough investigation through the interaction of HIFU with homogeneous tissue mimicking phantoms has been performed to further explain this mechanical effects and their role in opening the BBB.

1.3. **Objectives*:***

The objective in this study is mainly constructed into two parts. The first part is to develop and implement a non-invasive, fast, and spatially resolved temperature measurement method to detect the instantaneous temperature rise at the HIFU focal spot in water. Furthermore, the study will investigate the role of the acoustic streaming in water on the temperature of the focal point. Such a technique would be well suited to quantify heating from highly focused devices with shock formations. We propose the implementation of pulsed, planar laser induced fluorescence LIF as a non-invasive optical imaging tool for measuring fast temperature rises in water. In LIF, a trace amount of a temperature sensitive fluorescent dye such as Rhodamine or Fluorescein is dissolved with the water. When excited by a coherent light source (typically blue ~ green), the dye fluoresces by emitting a Stokes-shifted signal (typically orange ~ red). The intensity of the fluorescence emission depends on the dye solution temperature. One can then calibrate the fluorescence into a temperature signal in situ. The process of fluorescence is fast (~ 30 ns). If one also uses a short excitation pulse from a Q-Switched laser (e.g. 10 ns, Nd-YAG) then a fast <50 ns rise time temperature measurement tool is possible. This optical technique is non-invasive in nature, and only requires optical access to the HIFU focal spot. Generally the laser light is formed into a thin sheet such that a planar area of the fluid within the HIFU focal spot is illuminated, and the instantaneous temperature field is measured. Due to its fast response time, LIF thermometry has been successfully used to probe the fast varying turbulent water flumes in the wake of a heated cylinder (Seuntiëns et al. 2001) with a reported temperature resolution of 0.1 °C. This tool is well suited for HIFU studies where the domain of interest ranges from room temperature to near boiling. LIF has also been

calibrated as a concentration sensor in a fast varying turbulent flow (Winkel et al. 2009). A recent review (Crimaldi 2008) discusses various implementations of planar LIF as an optical diagnostics tool in fluids. Furthermore, the acoustic streaming in the focal point is studied and wither the streaming have any role on the temperature rise at the HIFU focal point. Particle imaging velocimetry (PIV) is proposed to quantify the acoustic streaming at the focal point of the HIFU as a non-invasive method to capture instantaneous velocities occurring at the focal point as ultrasound propagates through it.

The second part of the study is to study the mechanical effects other than thermal ablation denaturing and cavitation effects on tissue. Deformation and rapturing of pure homogenous tissue mimicking materials due to radiation force and stress fields will be experimentally investigated. Laser Digital Image Correlation LDIC technique to quantify the deformation of the tissue is proposed. LDIC is a technique that is very similar to PIV in fact it shares the same experimental setup. Furthermore, the formation of cavities and raptures in tissue is monitored and studied using conventional high speed imaging techniques at the focal point of HIFU.

CHAPTER 2

METHODS AND EXPERIMENTAL SETUP

Experimental study on the interaction of HIFU with propagation medium, such as water and tissue mimicking phantoms is investigated. Several setups and experimental methods are used. This chapter will start by illustrating the temperature output and shock induced heating in water is going to be pursued using Laser Induced Fluorescence Thermometry. The acoustic streaming effects in water and its role in the convective cooling of the focal spot is going to be investigated using Particle Imaging Velocimetry. The deformation inside tissue mimicking materials due to radiation force inside tissue is investigated using LDIC. The initiation of tears inside tissue and denaturing is going to be investigated using top and back illuminated imaging. Finally, the calibration setup used to calibrate the electrical input to the transducer to the acoustic power output at the water field by using Radiation Force Balance (RFB).

2.1. Laser Induced Fluorescence Thermometry of Pulsed HIFU:

A thin, pulsed laser sheet (8 ns pulse width) was used to excite the aqueous fluorescent dye solution present at the focal region of a spherically focused HIFU source. The temperature-sensitive fluorescence signal from the focal region was recorded using a CCD camera and was converted to an absolute temperature scale using in situ calibration. A schematic of the setup is shown in **Fig.3 (a)**.

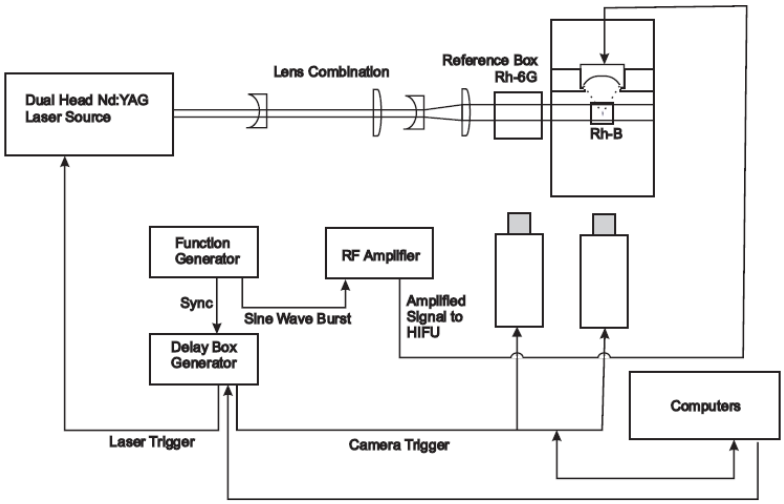

(a)

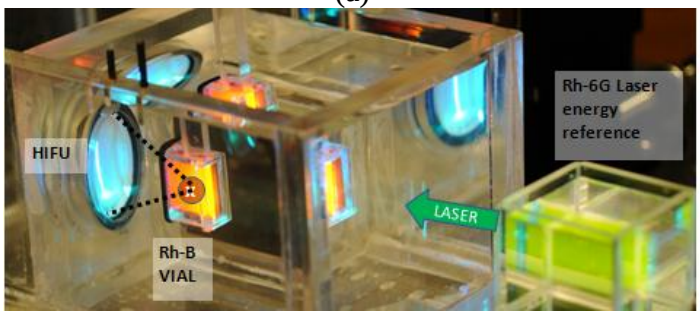

(b)

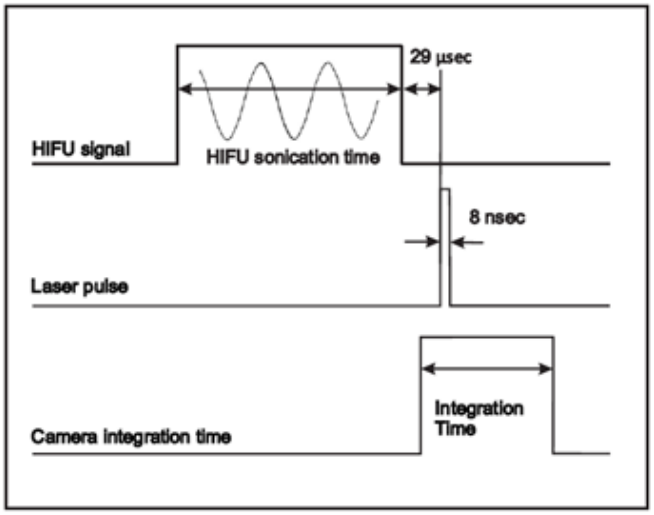

(c)

Fig. 5: (a) Schematic of the LIF setup (The same schematic works with the PIV and LDIC). (b) Image of the LIF setup and the fluorescence vail. (c) LIF timing schematic

2.1.1. HIFU Transducer

The HIFU transducer was an air-backed piezoceramic transducer with a 44 mm diameter, 44 mm focal length and was operated at 2.158 MHz. The transducer was driven using a function generator (Agilent 33250A) and a radiofrequency amplifier (Model A75, Amplifier Research, IL, USA). The transducer was an exact replica of the transducer used and characterized by Canney et. al. (2008). It exhibited nonlinear wave propagation at the local spot seen from the asymmetric pressure waveforms and the steep shocks at power intensities above 6,000 W/cm^2. For the current LIF experiments, the transducer was operated with pulse lengths between 0.125 ms and 10 ms, at HIFU focal intensities between 5,200 and 18,500 W/cm2.

2.1.2. Water Bath

The HIFU transducer was placed in a water-filled cast acrylic tank measuring 10×10×12 cm of 1 cm wall thickness. The HIFU source was mounted in the side wall of the tank and another hole was drilled in the other side wall of the tank and fitted with a glass window for passage of the laser to avoid the laser sheet burning the cast acrylic. The tank was filled with distilled water before experiments and left to run overnight through a submicron reverse-osmosis ceramic filter, and to degas using a 12-pin-hole degasser (Kaiser et al. 1995). The degassing system consisted of a water tank, a half a horse power circulating centrifugal pump, and a cylindrical polyamide casing having a cast-acrylic face. The polyamide casing was mounted to the suction side of the pump. After the distilled water is strained through the holes the water is passed to a ceramic filter. The water afterword is returned to the water tank. The degassing system is left to degas for at least 20 hours before operation the dissolved oxygen level is then measured

to be 1.8 ppm at 25 deg C using oxygen meter (Oximeter G-538, WTW Germany). This dissolved oxygen concentration enables us to separate any cavitation effects in order to get a pure temperature signal during the experiments.

2.1.3. Laser Induced Fluorescence LIF

An aqueous solution of a temperature-sensitive fluorescent dye (Rhodamine B, R6626, Sigma-Aldrich, St. Louis, MO) was degassed and placed in a 2×2×2 cm3 cast acrylic 4-sided vial with a wall thickness of 2 mm at a concentration of 10×10-6 M or 4.8 grams per cubic meter. The vial was co-located with the HIFU focal volume and two sides of the vial (perpendicular to the acoustic beam axis) were covered with a thin commercial cling film to contain the dye while minimizing disturbances to the passing HIFU acoustic beam. The Rhodamine dye was placed in a small vial instead of dying the whole bath to minimize the optical path lengths travelled by the green excitation light and the red emission light in order to minimize the effects of absorption and signal quenching from self-absorption. These absorption effects were minimized further by choosing a relatively low dye concentration level that produced a good signal-to-noise ratio, and by optimizing the laser power setting.

The dye was excited using a green laser beam from a pulsed Nd-YAG laser source (beam dia. 6 mm, 532 nm, 8 ns pulse width, 150 mJ/pulse max., Quantel-Big Sky, Montana, USA). The laser light was collimated by a pair of spherical lenses into a large 50 mm beam before it was formed into a thin light sheet, 0.3 mm thick and 6 mm wide, by a pair of cylindrical lenses (-50.8 mm and +250 mm) slicing through the HIFU focal spot normal to the acoustic axis. This arrangement produced a transverse section

visualization of the HIFU focal volume. Since the thickness of the light sheet (0.3 mm) was significantly smaller than the heated spot length of the HIFU (2~4 millimeters), negligible cross-sheet averaging artifacts occurred. We also attempted a case where the light sheet was aligned parallel to the acoustic axis resulting in a longitudinal section of the HIFU focal region.

The Stokes-shifted red fluorescent signal from the excited dye was imaged using a 12-bit gray-scale SensiCam SVGA digital camera (1024x1280 pixels, PCO, Germany). The camera's optical axis was set perpendicular to the laser sheet direction to image a field of view approximately 1.8×2.2 mm2 enclosing the HIFU focus. The camera front lens was custom fitted with a 550 nm long pass Schott glass filter (model LG 550, Thorlabs, NJ) which preferentially allowed the red LIF fluorescent signal to pass, but blocked out the green excitation light. The process of fluorescence excitation is fast and occurs over a period of approximately 30 ns and is therefore well-suited to handle the fast heating (here on the scale of a millisecond) associated with HIFU exposures.

The fluorescence intensity of Rhodamine B is linear with temperature and has been reported to drop with increasing temperature at an average rate of 1.58% per degree Celsius (Sutton et al. 2008). But, the temperature sensitivity of the dye can vary among studies depending on the solvent type, species concentration, laser source and detector specifications, as well as other experimental details and therefore was directly measured using in situ calibration experiment. The calibration involved static heating of the whole water bath from 20 ^{0}C to 30 ^{0}C (measured to within +/- 0.2 ^{0}C) using an electricl heater submersed in the water tank and regulated by a PID controller. A small (~10 W) circulation pump was used to circulate the water gently for temperature

uniformity across the tank. The setup, including the laser sheet, camera, and dye solution vial, was kept untouched between the HIFU exposure and the in situ calibration. Four to five temperature set points were used in the calibration within the range of interest. At each of the calibration set temperatures, a total of 50 LIF images were recorded and were then averaged to reduce random noise. The random noise was further reduced using 4×4 pixel binning. The resulting spatial resolution of the temperature measurements was 0.01 mm within the image plane. This resulted in 20~30 measurement points across the 200~300 micron thickness of the HIFU heated spot. For each individual pixel within the image, a linear curve fit was obtained, relating the temperature T to the LIF intensity I in the form $\boldsymbol{T = c_1 I + c_2}$; where $\boldsymbol{c_1}$ and $\boldsymbol{c_2}$ are constants. The intensity in this formula was also corrected for the laser input energy variations. Additionally, the calibration was done pixel by pixel to account for any spatial intensity variations within the light sheet, and possible spatial gain variations of the CCD pixels. A typical in situ calibration curve relating the LIF intensity to temperature is shown in **Fig.6**. The normalized fluorescence intensity drops by 1.36% per ^{0} C, which is within the typical range reported for Rhodamine B. The vertical bars indicate a +/- one standard deviation. The standard deviation also reflects that the calibration points shown in the figure are taken from averaging over a region of 85×225 pixels. The calibration uncertainty is estimated at 0.25 ^{0} C (95% confidence level). Three thermocouples were used during the experimentation to monitor the background temperature: one was placed directly in the water bath; the other was placed near the top part of the measurement vial to sense any variations associated with thermal plumes buoying up; and the third was placed near the center of an identical mock water vial placed near the corner of the water bath. All three temperatures agree to within 0.2

degrees, and the measurement vial thermocouple did not indicate any statistically significant variations in the background temperature during the HIFU irradiation.

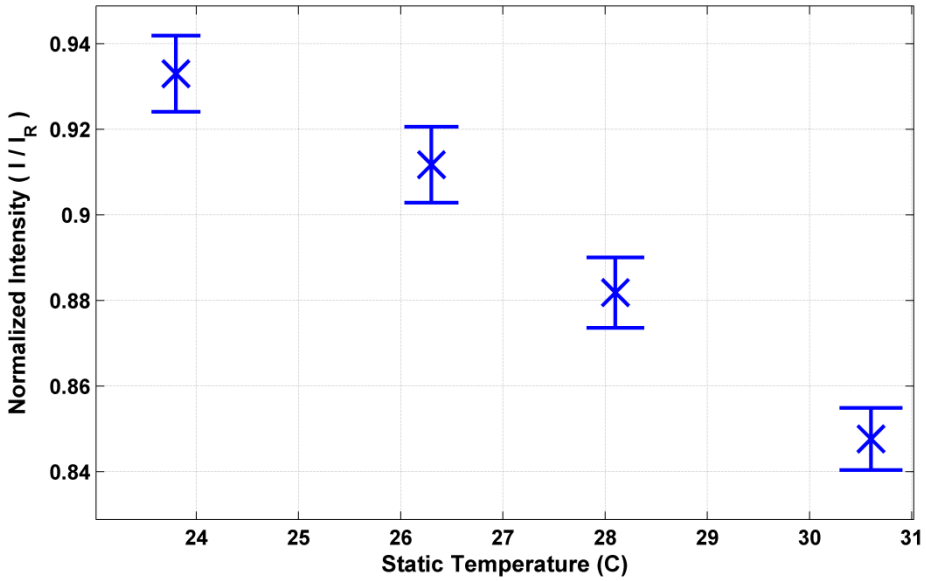

Fig. 6: Sample calibration curve of water averaged over 225×85 pixels

To measure the pulse-to-pulse laser energy variations, the collimated laser sheet was passed through a reference cuvette of constant temperature before entering the water bath. The cuvette contained a uniform aqueous solution of Rhodamine 6G fluorescent dye (R4127, Sigma-Aldrich, St. Louis, MO). This fluorescence intensity was imaged using a second identical CCD camera to provide a measurement of the laser pulse energy before entering the HIFU water bath. The fluorescence of Rhodamine 6G, unlike Rhodamine B, is not sensitive to temperature. The reference cuvette was covered to prevent evaporation of the dye. The reference-beam-energy CCD recorded the spatial distribution of the laser pulse energy. The specific portion of the beam used to illuminate the HIFU focal spot was marked to allow the mapping of the laser reference energy to the actual LIF measurement. This was then used to correct for the input light intensity in the LIF recordings.

By using a master trigger and a time delay from a timing unit (Delay Generator DG100N, Thorlabs, NJ), the temporal delay of the laser excitation pulse relative to the HIFU burst could be adjusted to acquire the LIF thermometry signal at different relative timings. The synchronization scheme was implemented through an in-house program written using LabView (National Instruments, Austin, TX). A demonstration of the timing scheme is shown in **Fig.5** (c).

We report two sets of HIFU burst measurements; in the first set, the HIFU was triggered to provide a short burst, and precisely at the end of the burst the LIF thermometry laser is fired. The delay takes into account the travel time of the sound wave to reach the focal plane. The burst length was varied from 270 cycles (0.125 ms) up to 21,580 cycles (10 ms). In the second set of experiments, the HIFU was triggered to give a burst of 10 ms, and the LIF thermometry laser was triggered to fire at pre-determined delays after the initiation of the HIFU burst. The same delays as in the first set of experiments were used. In each of the experiments, between 70 and 100 instantaneous LIF thermometry images were taken at each delay to gain statistical information on the behavior of the heated spot. There was a delay of 5 to 10 seconds between consecutive instantaneous HIFU bursts in order to ensure there was no significant effect from preceding HIFU pulses on the current measurement point.

2.2. Particle Image Velocimetry of Pulsed HIFU in Water:

In addition to LIF measurements, particle image velocimetry (PIV) was also performed to determine whether acoustic streaming could lead to convective cooling and affect the temperature measurements recorded using LIF. PIV was used as a non-invasive, instantaneous, flow field velocity measurement within and around the HIFU

focal spot. To perform PIV measurements, the same laser sheet/imaging hardware and setup was used as in LIF, though PIV and LIF were not operated simultaneously. With PIV, the pulsed light sheet was oriented to cut longitudinally; i.e. parallel to the acoustic beam axis in order to visualize the streaming velocities. The camera was operated in the cross correlation mode, in which two separate image frames (image pair) were acquired with an inter-frame timing controllable down to 0.2μs. The dual-head laser was used to provide two consecutive 8 ns pulses to illuminate the image pair. Titanium dioxide nano-particles (100 nm, cat# 677469, Sigma Aldrich) were added as flow tracers to the water vial after a sifting treatment aimed at reducing the average particle size. The particles were dually illuminated by the laser sheet and imaged on separate frames with the CCD camera. We tested the tracer settling time where the water vial containing the particles was placed in the PIV measurement setup, and left in situ for many days unperturbed and unshaken; images of the particles were taken before and after. The density and size of particles in the images (no flow or perturbation) remained unchanged over many days, indicating that the tracers have a long settling time, and would act as faithful tracers of the flow. Moreover, during HIFU exposure, the particle density stayed uniform and no concentration/depletion patterns could be discerned in the images from the mean acoustic streaming or the acoustic particle velocity.

For the PIV measurements in water, the HIFU source was operated at 14,000W/cm^2 focal intensity. The PIV was triggered to capture the velocity field at controllable time delays after the end of the HIFU burst. The used PIV inter-frame timings ranged between 3μsec and 20μsec. Thirty image pairs were acquired for each case to generate average vector fields. A wait of roughly 10 sec was applied between any two consecutive HIFU bursts to allow for the motion from the preceding burst to

dissipate. The residual velocity prior to PIV imaging was estimated at a few mm/sec which was negligible relative to the HIFU acoustic particle velocity and streaming velocity O(m/s). The image pairs were processed with the PIVLAB-2000 Matlab software developed by Han and Mungal (2003) using a desktop computer. An interrogation window of 32 pixels and 50% overlap was used to generate a vector field with 77 by 61 vectors, at a vector spacing of 27μm thus allowing the resolution of 8 ~10 vectors across the thickness of the HIFU heated spot. Vector post filtering was used to identify and replace outliers in the field based on comparing each vector to its surrounding grid neighbors. Typically, 2~3 % of the vectors were identified as outliers and replaced through interpolation.

2.3. Pulsed HIFU Laser Digital Image Correlation and High speed imaging in Clear Tissue Mimicking Phantom:

LDIC experiments were performed on RTV-615 rubber as a clear tissue mimicking material that has been reported to have near to body properties (Maggi, 2009). The experiments aimed to measure the deformation in the tissue mimicking phantom due to radiation force. LDIC was used as a non-invasive, instantaneous, radiation force displacement field measurement within and around the HIFU focal spot. To perform LDIC measurements, the same laser sheet/imaging hardware and setup was used in the same way used with the PIV in water experiment. In this experiment, the pulsed light sheet was oriented to cut the cross-section and through the focal spot; i.e. perpendicular and parallel to the acoustic beam axis. The parallel configuration makes us able to so the axial deformation due to the radiation force. The perpendicular configuration will make the radial deformation due to the radiation force available for

measurement. The camera was operated in a standard mode, in which exposure are integrated into a single frame. The first image integrates the first laser pulse before any HIFU insonification. The second image integrates the pulse at the end of the HIFU insonification. The dual-head laser was used to provide an 8 ns pulse to illuminate the images. Titanium dioxide nano-particles (100 nm, cat# 677469, Sigma Aldrich) were added as displacement tracers to during the mixing process of the RTV-615 tissue mimicking phantom.

The LDIC measurements in RTV, the HIFU were done under HIFU focal intensities in the range of 2,500 to 18,400 W/cm^2. The PIV technique was used to determine the displacement due to HIFU exposure. Final displacement field was obtained from five instantaneous displacement fields. Each of the displacement fields was exposed on a virgin material, to insure that there is no effect due to the prior HIFU exposure. Furthermore, a different random configuration of the tracer particles will be used in each displacement field image pairs to insure that the particle do account for the displacement in the field. Also, it would compensate for any loss of information at any part of the vector field due to the random particle distribution. The image pairs were processed with the PIVLAB-2000 Matlab software in the same way with the water PIV experiment. An interrogation window of 32 pixels and 50% overlap was used to generate a vector field with 77 by 61 vectors, at a vector spacing of 28μm thus allowing the resolution 35 vectors across the thickness of the deformation region at the focal point radially.

In order to determine at which power and insonification duration does rapture happen in RTV-615, and to understand the mechanism of growth of the rapture. High speed imaging using back and top illumination is used. The RTV-615 gel was casted in

rectangular cast-acrylic rectangular boxes with the dimensions of $2 \times 3 \times 3.5\ cm^3$. The mixture was held under strong vacuum until no traces of bubbles is found in the mixtures. A 500 W white light source was used to illuminate as top or back illumination in order to visualize the micro sized cracks. A PCO camera was used in standard mode in order to capture images at the end of the burs to determine of the length of burst at a certain power was able to cause the rapture in the tissue mimicking phantom. The high speed camera (Phantom v9.1, ResearchVision USA) was used to understand the initiation and the growth of the rapture in the tissue mimicking phantom. The camera was operated up to 13,029 fps at a resolution of 152x704 pixels.

2.4. Calibration of HIFU Transducer Using Radiation Force Balance:

The HIFU is mounted in a water bath such that the axial direction of the ultrasound path was upwards. The water bath has the dimension of 14×14×11 cm consisting of a 5 mm thick wall. The housing for the HIFU was machined using precision CNC machine setting the focal point to be 40 mm above the bottom of the water tank. An acoustic absorbent rubber (NPL - HAM A Acoustic absorber, UK) was suspended 1 cm away from the HIFU face an additional weight of 37 grams was held over the acoustic absorber. Analytical balance (A&D G-200, Tokyo Japan) was connected to computer to log weight difference as the insonification take place. The Function generator was set to continuous mode for 3-5 seconds repeatedly for several bursts. The signal was processed in MATLAB and converted the mass change to Acoustic power using the equation $P = c_s.\Delta m.g.\frac{2}{(1+\cos\gamma)}$, such that c_s is the speed of sound in the medium of propagation, and $\measuredangle m$ is the difference in mass caused by the

ultrasound transducer, g is the gravity acceleration, and γ is the half focusing angle of the ultrasound transducer. **Fig.7** shows pictures and schematic of the RFB calibration setup. The operation voltages calibrated are in the range of 35 – 319 Vpp.

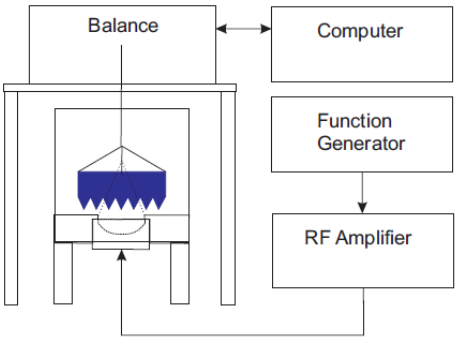

Fig. 7: Radiation Force Balance calibration setup schematic

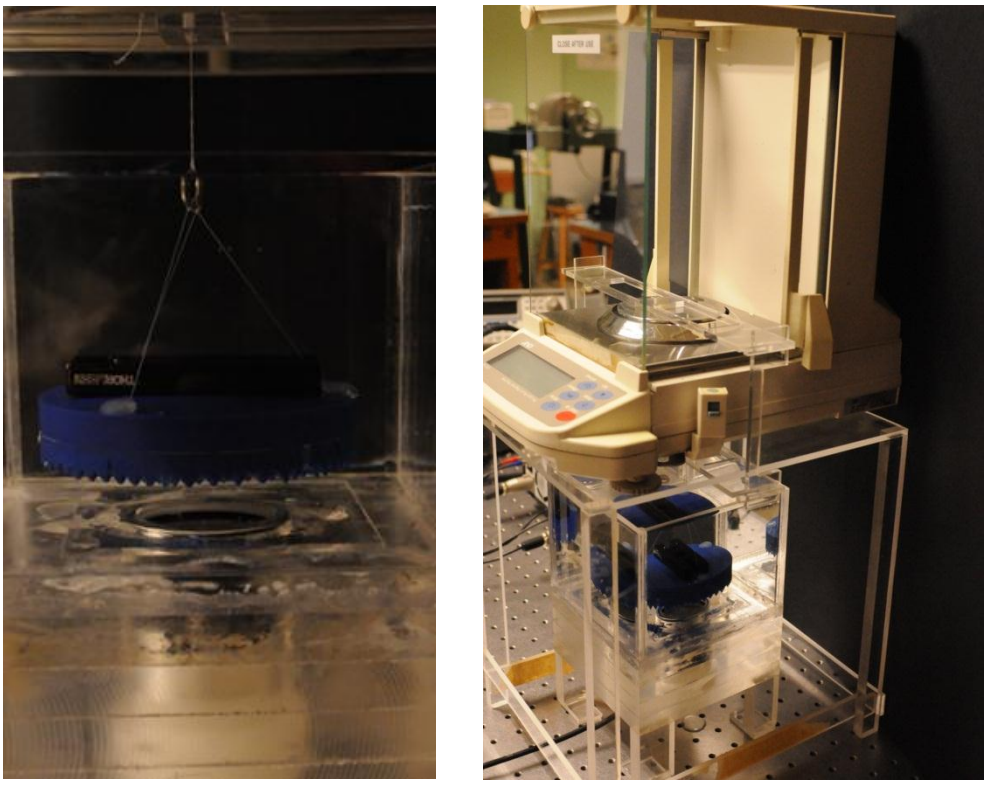

Fig. 8: Images of the Radiation Force Balance Calibration setup

There are several problems associated with the radiation force balance setups in terms of getting the right acoustic power of the transducer. One of the problems is the heating of the acoustic absorber which leads to the floating of the absorber causing an over estimation of the acoustic power. Mainly the relation between the acoustic power determined by the RFB, and the RMS of driving fundamental voltage (input Electrical Power) of the HIFU is linear. In other words, the relation between the fundamental peak to peak voltage and the acoustic power is quadratic. The heating bias in the experiment is only pronoun at highly powers. At these high powers it is very easy to distinguish the biased points as outliers (Canney et al., 2008). The linear relation is easily noticeable at the low power operation. Furthermore the few points that are biased in the curve can be estimated by the relation determined by the low intensity points, which make 70% of the curve. To be able to calculate the Spatial Averaged Intensity (I_{SAL}) the acoustic power output is divided by the area of the cross-section of the focal spot at -6 db that is determined by a hydrophone. The HIFU transducer used and characterized by (Canney et al.,2008) is a replica to the transducer used in this study. The area of the -6 db focal is used from the Canney et al paper to determine the I_{SAL} was measured to be 0.1 mm.

CHAPTER 3

RESULTS

In this chapter the results from the experiments made using the HIFU to study the mechanical effects associated with the interaction between the focused acoustic waves and the propagation medium (water, Tissue mimicking phantom).

3.1. Laser Induced Fluorescence Temperature Measurement:

Fig.9 shows a LIF image with the laser sheet slicing the HIFU heated volume longitudinally (parallel to the acoustic axis)**.** The HIFU transducer was operated using a single burst of 10 ms length, and the LIF laser was fired 9 ms after the onset of the HIFU burst. The spherical focusing of the HIFU beam can be observed in the repeating intensity pattern seen in the snapshot, **Fig.9 (a)**. The pattern spacing is ~ 0.69 mm and it matches the wavelength associated with the 2.158 MHz HIFU frequency. The focal spot of the HIFU is identifiable as well. This image is akin to the shadowgraphy technique used for shock visualization (Brujan et al. 2011). But, it is enhanced here by the use of the fluorescent dye, which makes the detection of the laser intensity within the fluid easier. Yet this is different from Schlieren imaging (Neuman and Ermert 2006) often used in HIFU labs which uses light diffraction from a knife's edge for signal detection. For **Fig.3 (b)**, by timing the laser to fire just after the HIFU acoustic wave has moved away from the focal spot, the refraction pattern would not be present in the image. Only when the laser and the sound meet is this pattern discerned. There is also a dark elongated part near the focal region resulting from a reduction in the laser-induced

fluorescence intensity in that region because of the localized temperature rise from the energy deposited by the HIFU, confirming the HIFU heating in water.

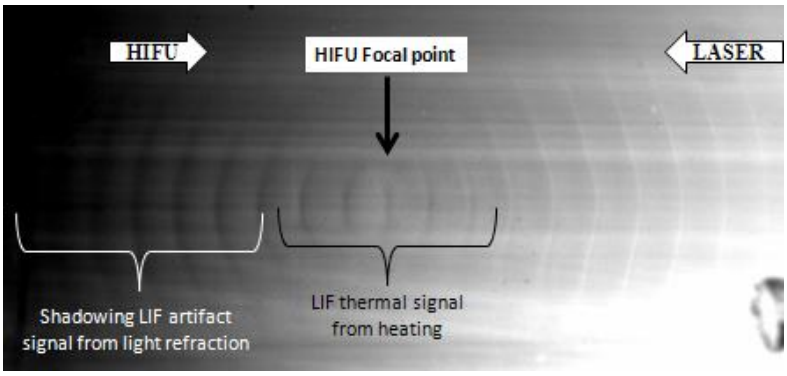

(a)

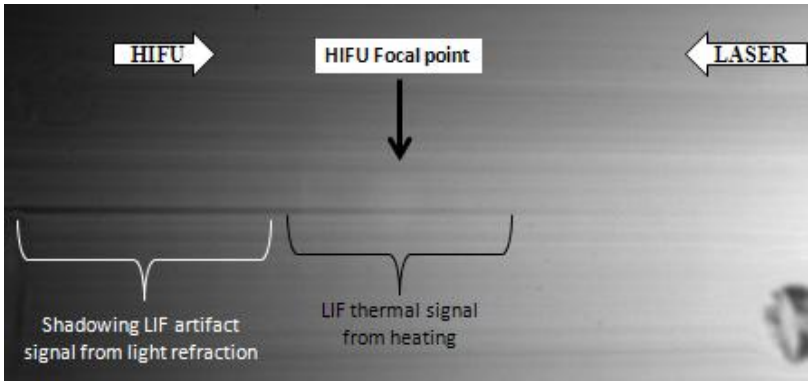

(b)

Fig. 9: (a) Longitudinal cut through HIFU focal spot shows spherical focusing waves that matches the 0.69 mm wavelength - 10 ms pulse at 14,000 W/cm^2 the cut was taken 9ms within the 10 ms burts. (b) Longitudinal cut through HIFU focal spot shows shadowing artifact after a 10 ms pulse at 14,000 W/cm^2

Additionally, an optical thermal lensing region appears behind the heated region as a shadow and is roughly marked in the figure. The heated spot with the thermal lensing shadow appear as a continuous elongated dark spot, yet it should be noted that the heated region is only a small part of this and the rest is an optical artifact

from the index of refraction mismatch across the temperature interface. As the laser light refracts near the heated spot, it deflects, creating a darkened pattern in its wake, or the thermal lensing shadow. This shadow is the integral effect of a continuous series of light refractions across the temperature gradient (refractive index gradient), and its extent and strength depend on the size/geometry of the temperature gradient region as well as on the magnitude of the temperature gradient itself. A larger-sized hot spot and a larger temperature gradient will result in a more pronounced thermal shadow effect. The detection of the thermal lensing in these experiments is made possible by the presence of the fluorescent dye which acts as a marker of the laser beam energy passing through a given region. Rotating the light sheet orientation by 90° to intersect perpendicularly to the sound beam, and sweeping it across the heated region reveal that the heated liquid region is around 3 ~ 4 mm in length. The peak temperature observed in this study is 4 °C at the highest power level used.

In order to separate the LIF temperature signal from the thermal lensing artifact, we have experimented, in addition to the temperature sensitive Rhodamine B dye, with Rhodamine 6G, which is not temperature sensitive. With Rhodamine 6G, the only effect that could be observed is the thermal lensing shadow from the light refraction effect in the wake of the heated spot, while there is no fluorescence drop signature from the heated spot itself. **Fig.10** shows the results from this trial. The light sheet cuts perpendicular to the HIFU beam near the focus. The laser was fired only a few microseconds after the passage of the last HIFU wave to avoid capturing in the image the spherical pressure wave shadowgraphy pattern seen in the previous image. With both fluorescent dyes, the thermal lensing shadow behind the heated spot was present. However, in the sensitive Rhodamine B case, the darkened LIF signature due to

the temperature rise at the heated spot is present; while there is no LIF signature due to temperature from the insensitive Rhodamine 6G case. This clarifies the distinction between the LIF temperature signal, and the thermal lensing optical artifact. The cross sectional LIF image indicates that the width of the heated spot is approximately 0.2 ~ 0.3 mm.

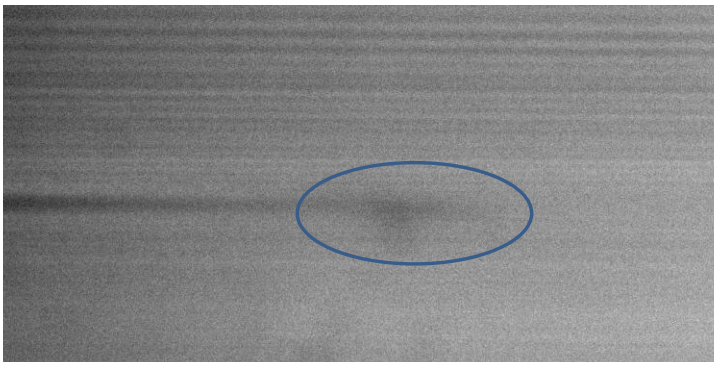

(a)

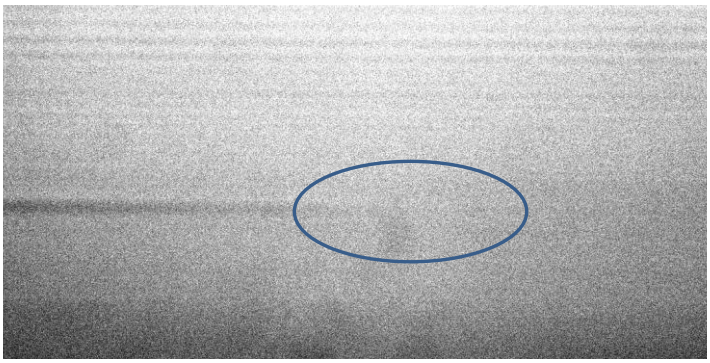

(b)

Fig. 10: (a) Rhodamine B temperature dependent intensity dye sonicated showing the dye intensity decreasing at the focal point due to the temperature increase at the focal spot along with the shadowing artifact. (b) Rhodamine 6G temperature independent day show

A simple light ray tracing model similar to the one described by Chehouani and Elmotassadeq (2009) was implemented using Matlab® (MathWorks, MA) to test how a localized temperature gradient in water, emulating the localized heat deposition by

HIFU at its focal volume, would affect a collimated, parallel light sheet passing through it. The light sheet is prescribed by many parallel, horizontal rays coming from the right side of the heated spot, **Fig.11**. The temperature of the heated spot is prescribed by a non-axisymmetric elongated Gaussian distribution $\boldsymbol{T(x,y) = T_0 e^{-(\frac{x^2}{R_1^2}+\frac{y^2}{R_2^2})}}$ **, Fig.11 (a)**, with peak temperature T_0 = 5 °C and an elongation factor $\frac{R_1}{R_2} = 5$ to reflect the 'cigar' shape of the HIFU heated volume. The index of refraction of the water far away from the heated spot is taken as *n = 1.3330*, while the temperature dependence coefficient of *n* is taken as $-1x10^{-4}$ per °C as estimated from Burnett and Kaplan (2004). A light ray will deflect according to Snell's sine law of refraction when encountered by a change in the refractive index of the medium along its travel path (just like a glass lens). By integrating the infinitesimal deflections of the ray, its path can be computed. To reproduce a light intensity map similar to LIF, the simulated pixel intensity at a given spatial location is assigned a value directly proportional to the number of rays passing through that location. This simple model shows indeed a thermal lensing region behind the heated spot of reduced light intensity, **Fig.11 (b)**, and it is generally consistent with the thermal lensing seen in the experimental LIF observations, **Fig.9**. The lensing is depicted by a dark area engulfed by two bright regions in the wake of the heated spot. The light rays are hence spatially re-distributed due to the thermal lens. Yet, it should be noted that the idealized two dimensional temperature distribution utilized with the ray tracing method may not precisely reflect the actual three dimensional shape of a HIFU heated spot. Also, water impurities, when present in general, can create noise in the index of refraction of the medium, which in turn would induce additional deviations from the modeled picture.

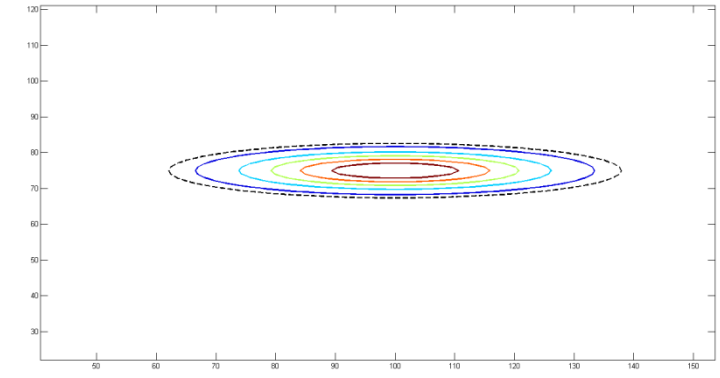

(a)

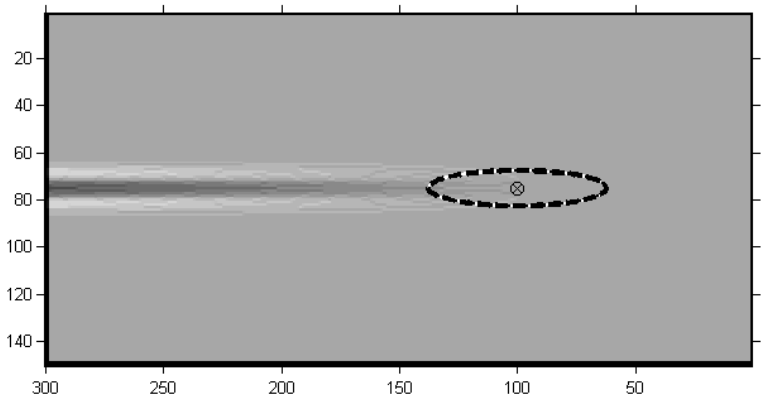

(b)

Fig. 11: (a) Heated sport temperature distribution , with Gaussian profile (b) numerical model of the heated spot shows shadowing artifact.

By scanning the laser light sheet to cut normal to the sound path at multiple axial locations one can gain information about the tomography of the heated spot. **Fig.12** presents transverse sections taken in water with 10 ms HIFU bursts (174 V_{pp}; focal intensity roughly 7000 W/cm2). The HIFU heated region shape changes and distorts in the axial direction with increased distance from the HIFU. PIV results discussed later indicate that acoustic streaming is strong post focal even with only 2~3 ms bursts. From these sections, the length of the heated spot is estimated to be 3~4 mm,

and its width to be 0.25 mm. This is consistent with the heated length estimation by Canney *et al.* (2010). Calibrated temperature data in water is presented next.

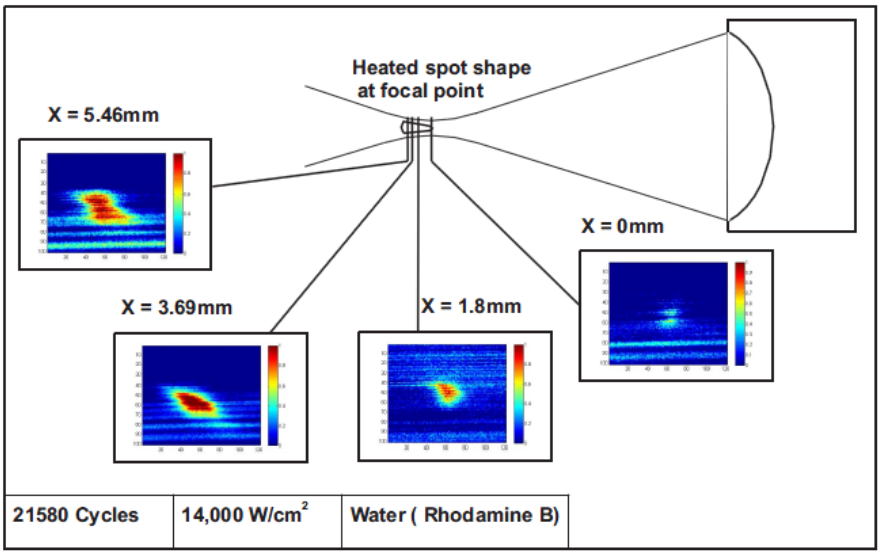

Fig. 12: Cuts through the heated spot show non-calibrated intensity images to show the shape of the heated spot.

Fig.13 shows the temperature fields (water and 20% Glycerin solution) at the end of four different lengths of HIFU bursts. Each of the four temperature fields is the average of ~ 90 instantaneous fields. The transverse cross sections show a nearly round heated region for the shorter burst, which can be noted to deviate from the circular shape with increased length of burst. The development of the non-symmetry in the heated region shape is thought to be caused by the development of acoustic streaming. PIV indicates that strong streaming in the focal spot region can develop within only a couple of milliseconds of the burst onset. Hariharan et al (2008) have noted that flow instabilities developed in water during steady acoustic streaming. Flow instabilities may be at action in our experiments as well leading to the observed shape asymmetries. The figure shows also that the temperature peaks around 3 ms after the burst initiation.

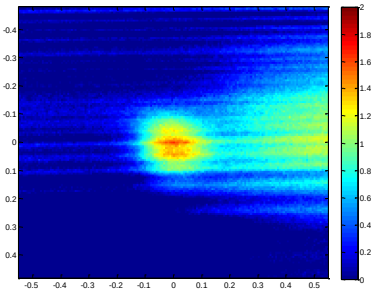

(a) 1079 cycles at 14,000 W/cm^2

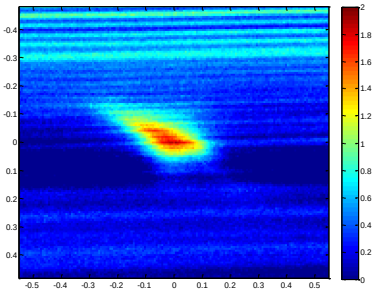

(b) 6474 cycles at 14,000 W/cm^2

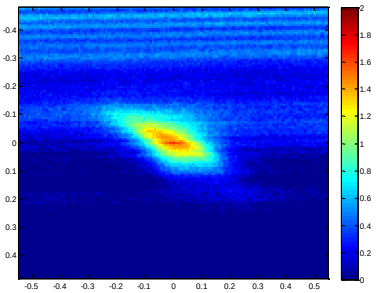

(c) 17264 cycles at 14,000 W/cm^2

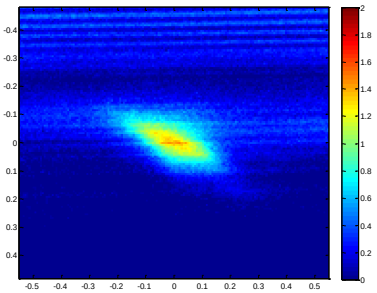

(d) 21580 cycles at 14,000 W/cm^2

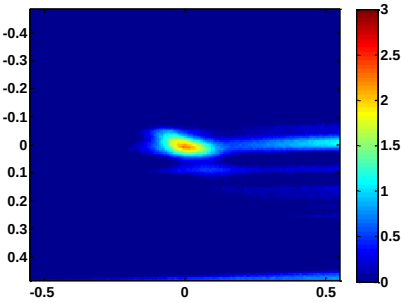

(e) 1079cycles at 14,000 W/cm^2

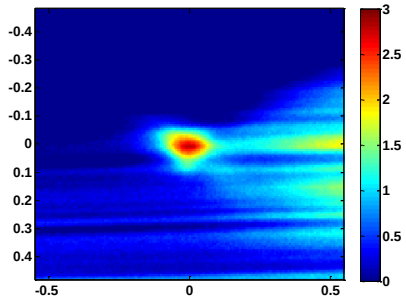

(f) 6474 cycles at 14,000 W/cm^2

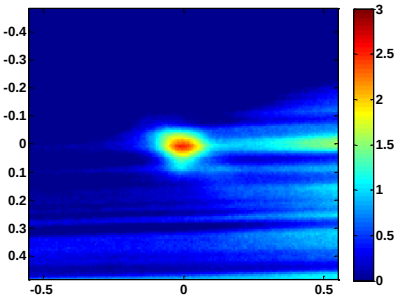

(g) 17264 cycles at 14,000 W/cm^2

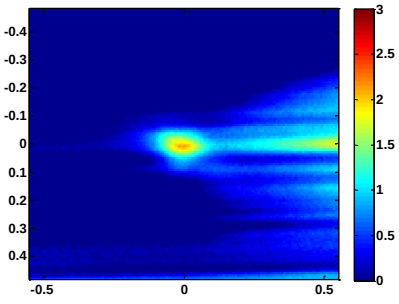

(h) 21580 cycles at 14,000 W/cm^2

Fig. 13: Temeprature field deteremined by LIF experiments of the cross section of the HIFU in water and 20% gly. solution with RhB at 14,000W/cm^2 (a,b,c, and d are in water, while e,f,g, and h are in 20% Gly. solution)

The linear temperature profiles confirm this observation in **Fig.14** which shows cuts in the temperature rise taken along the acoustic axis. The vertical bars label the ± one standard deviation as computed from 90 instantaneous measurements. It is interesting to note that the rise in temperature mostly happens within the first 500 μ *sec* in the burst (rate of heating 5000~6000 °C per second), while it takes another ~3000 μ *sec* for the temperature to peak. One can also detect the thermal lensing artifact in the linear profile by noting the trailing off patterns of the temperature rise with radial distance. The right-sided trailing off pattern (distal from the laser source, i.e. behind the heated spot) shows an upward temperature shift. The temperature signal is inversely proportional to the LIF fluorescence intensity. The thermal lensing effect increases with increasing focal temperature. As noted in the experimental method section, the experiments could be done in two ways. In one, the HIFU burst is fixed at 10 ms while the LIF thermometry is triggered at varying times from the burst onset. The other way is to fire the LIF thermometry at the end of the burst and vary the burst length. Data from the two methods are shown in **Fig.15 (a)**. It is not surprising that there is no statistically significant difference in the results from the two measurement modes. In **Fig.15 (b)** the effect of adding Glycerin to the water shows a significant temperature rise. Adding Glycerin will enhance the acoustic absorption of the water solution and increase the viscosity that will lead to less convective cooling effect on the heated spot. The effect of the HIFU input voltage on the focal temperature rise is considered. **Fig.16 (a)** shows the temperature rise with the number of cycles for two focal intensities of *14,000* and *18,500 W/cm*^{2}. The *initial* rate of temperature rise increases with increasing the input voltage to the HIFU, i.e., takes less time to achieve the same temperature rise with a higher input voltage. This suggests that even though the convective streaming effect

might be increasing with the source voltage alongside with the increase in heating, the net effect would be to cause a rise in the water temperature.

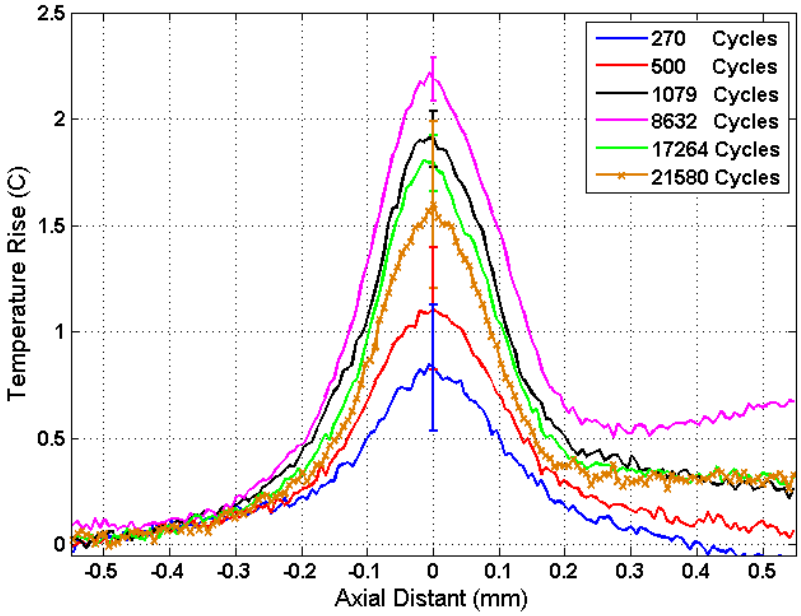

Fig. 14: Temperature profile though radial cuts for different sonication exposures.

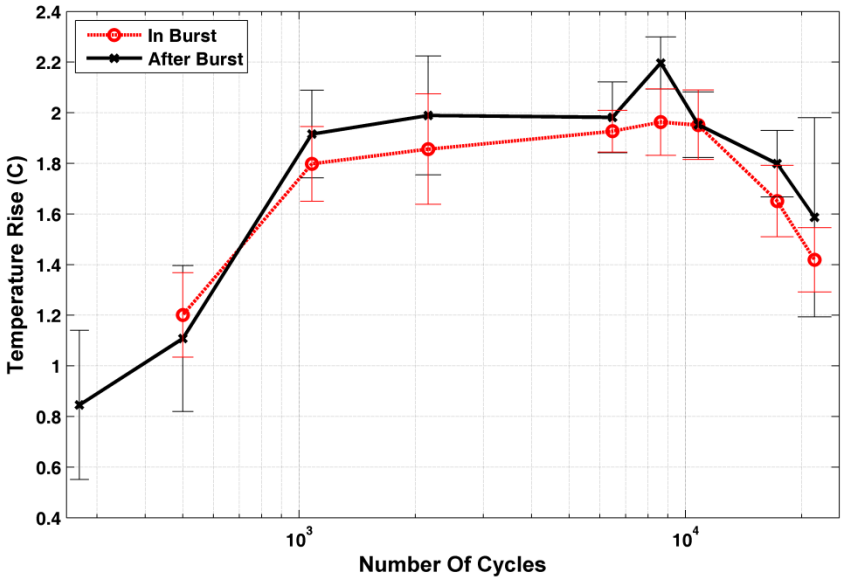

(a)

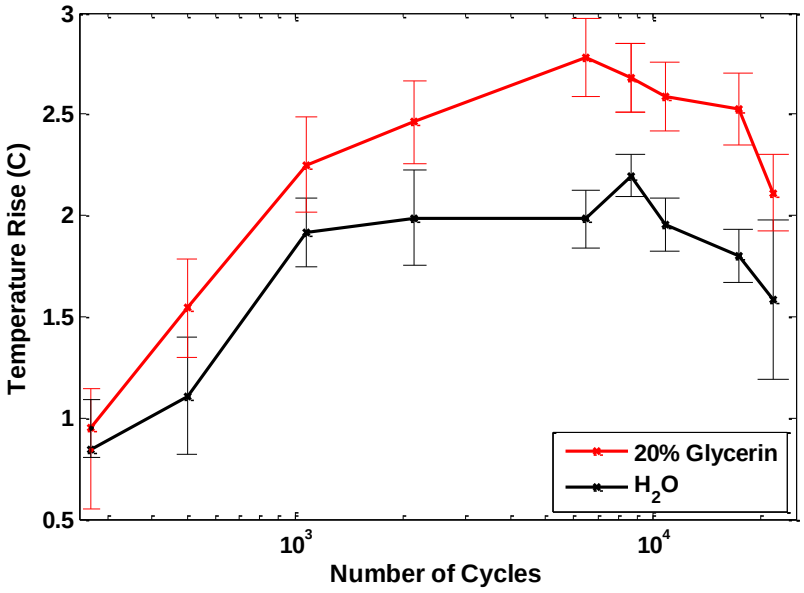

(b)

Fig. 15: (a) Temperature rise vs. number of cycles in two bursting methods in water-RhB solution. (b) Temperature rise vs. Number of cycles for (Water and 20% Gly. - RhB Solutions at 14,000 W/cm2)

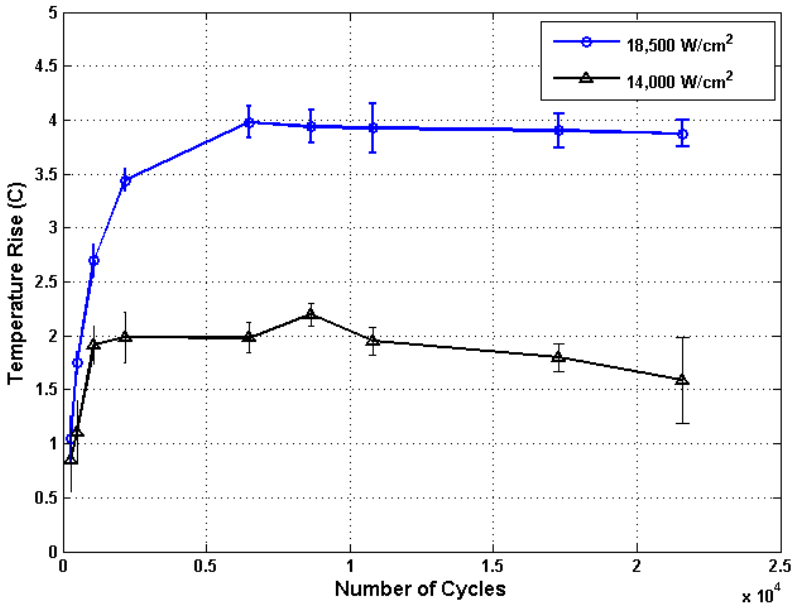

(a)

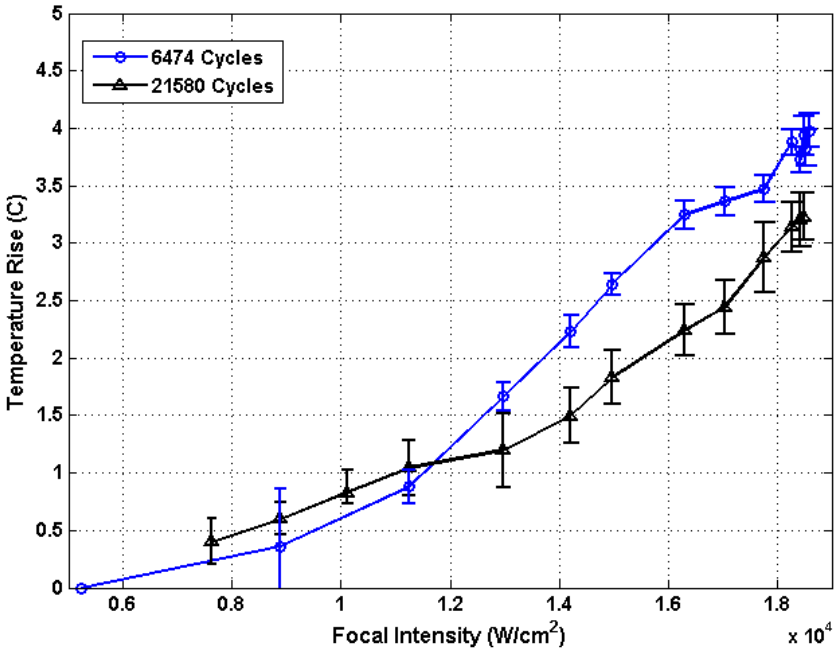

(b)

Fig. 16:(a) Temperature rise vs. number of cycles for operating focal intensities of 14,000 and 18,500 W/cm2. (b) Temperature rise vs. operating peak to peak voltage for two number HIFU exposure (3-10 ms)

Moreover, within the first few hundred microseconds of the burst, the heating rate can be inferred to be in the range of 4000 to 7000 degrees per second. **Fig.16 (b)** summarizes the effect of the input voltage on the instantaneous temperature rise for two burst lengths. It is clear that increasing the source voltage results in an increase in the focal temperature and in the heating rate; while increasing the number of cycles in a burst does not necessarily induce more heating, but in fact it can cause a lowering of the heating rate. It has been speculated earlier that acoustic streaming could be playing a significant role, and may be responsible for the reduction in heating rate with increasing burst length, as well as in the deviation of the shape of the heated cross section from axis symmetry.

3.2. Acoustic Field Velocity Measurements in Water:

PIV measurements were used to quantify the streaming velocities. An averaged PIV velocity vector field from 30 instantaneous realizations, with 3 ms HIFU single bursts is shown in **Fig.17** at 0.5 ms delay after the end of the sound burst. The PIV firing was delayed until after the passage of the sound burst to avoid capturing the acoustic particle velocities with the mean streaming motion. The streaming is clear and it is shown to intensify post-focal as the velocity magnitude increases with distal position along the acoustic axis. Also shown is a scatter plot of the instantaneous axial velocity component with radial distance from the acoustic axis taken near the downstream end of the vector field. The instantaneous scatter plot data are shown for the region marked by the dashed vertical lines in the vector fields. The average streaming velocity along the acoustic axis post-focal is (~ 1 m/s), while the instantaneous velocity data scatter is shown to exceed 2 m/s. Similarly for other burst lengths, the average streaming velocities were measured to be 0.02 m/sec for a 0.125 ms burst; and 0.6 m/s for a 2 ms burst. This indicates that streaming is initially weak but it intensifies with increasing length of burst. When the PIV was triggered to fire close to the end of the HIFU burst, the oscillatory acoustic particle velocity from the sound waves passage was quite strong and obscured the mean streaming motion.

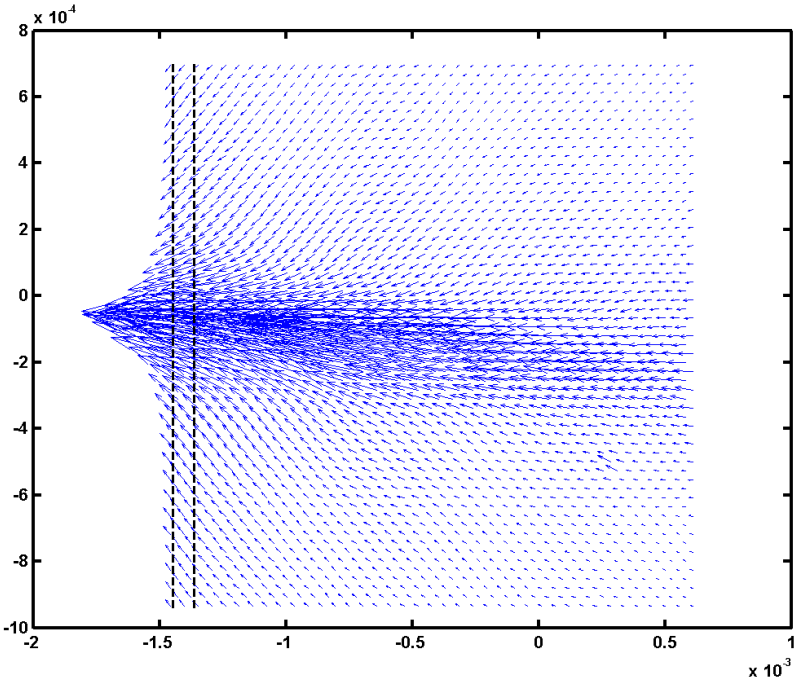

(a)

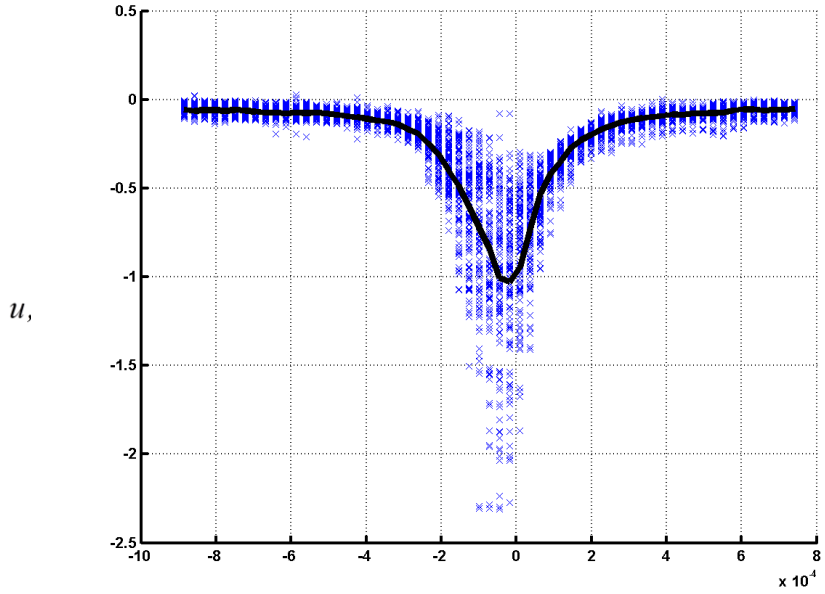

(b)

Fig. 17: (a) vector field of a 3ms HIFU burst delayed by 0.5 ms after burst at 14,000 W/cm^2 focal intensity. (b) cut through the vector field as indicated in fig.17 (a).

3.3. Tissue Mimicking Phantom Rapture and Deformation Experiments:

Fig.18 shows an image a sample tears formed in tissue mimicking material RTV-615 caused by pulsed high intensity focused ultrasound operated at a focal intensity of 18,300 W/cm^2. The experiment was operated at focal intensities in the range of 2,500 – 18,300 W/cm^2. **Fig.19** shows a scatter plot of the tear length vs. the operating power for different pulse exposures durations.

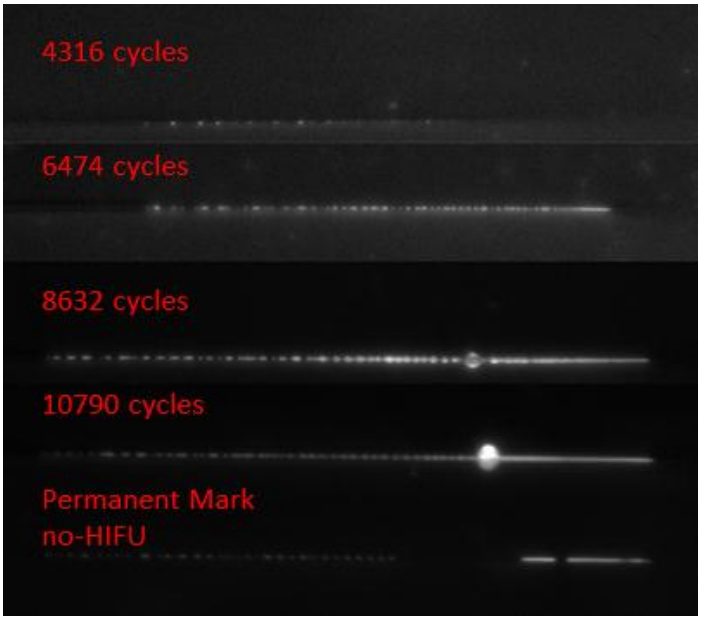

Fig. 18: Top illuminated RTV-615 tissue mimicking material exposed to pulsed HIFU at 18,300 W/cm^2 using PCO integrated image frame mode

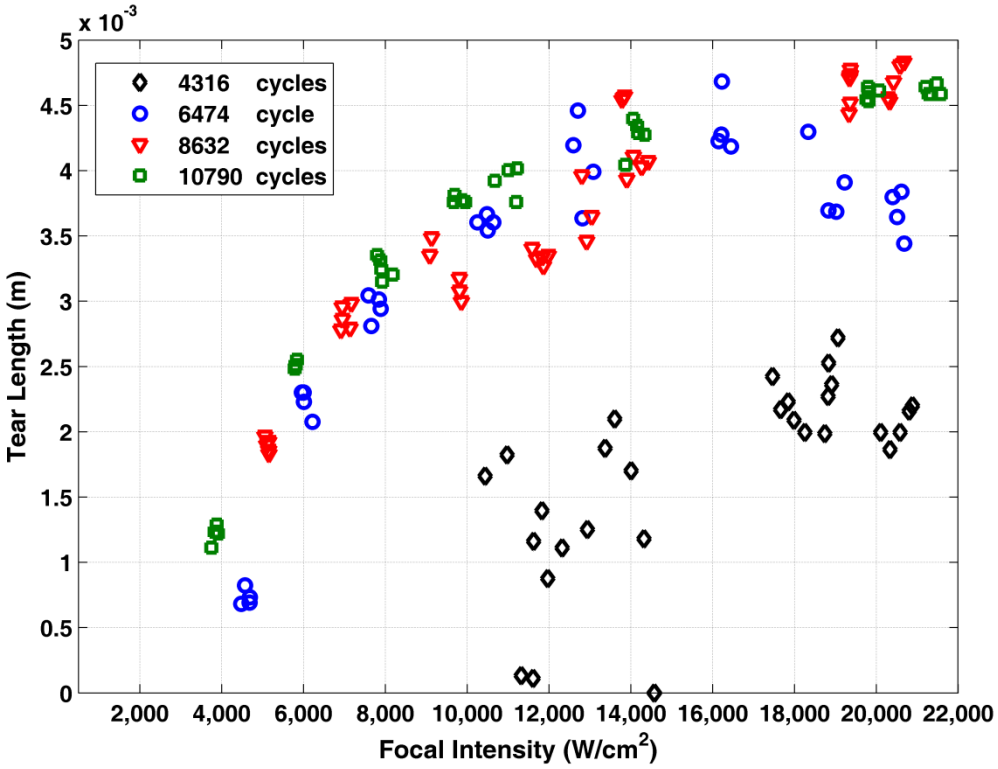

Fig. 19: Scatter plot of tear length vs. focal intensity of pulsed HIFU at exposures between 4316 and 10790 cycles.

It is clearly observed that below 2,000 W/cm^2 focal intensity there is no sign of any mechanically formed gaps/tears. High speed imaging was used to determine how the tear would initially start and grow. **Fig.20** shows the initiation and growth of the tear using back illumination. The camera was capturing images at 13,029 frames per second. The HIFU pulse was operated at a focal intensity of 18,500 W/cm^2 and a HIFU exposure of 10790 cycles (5 msec).

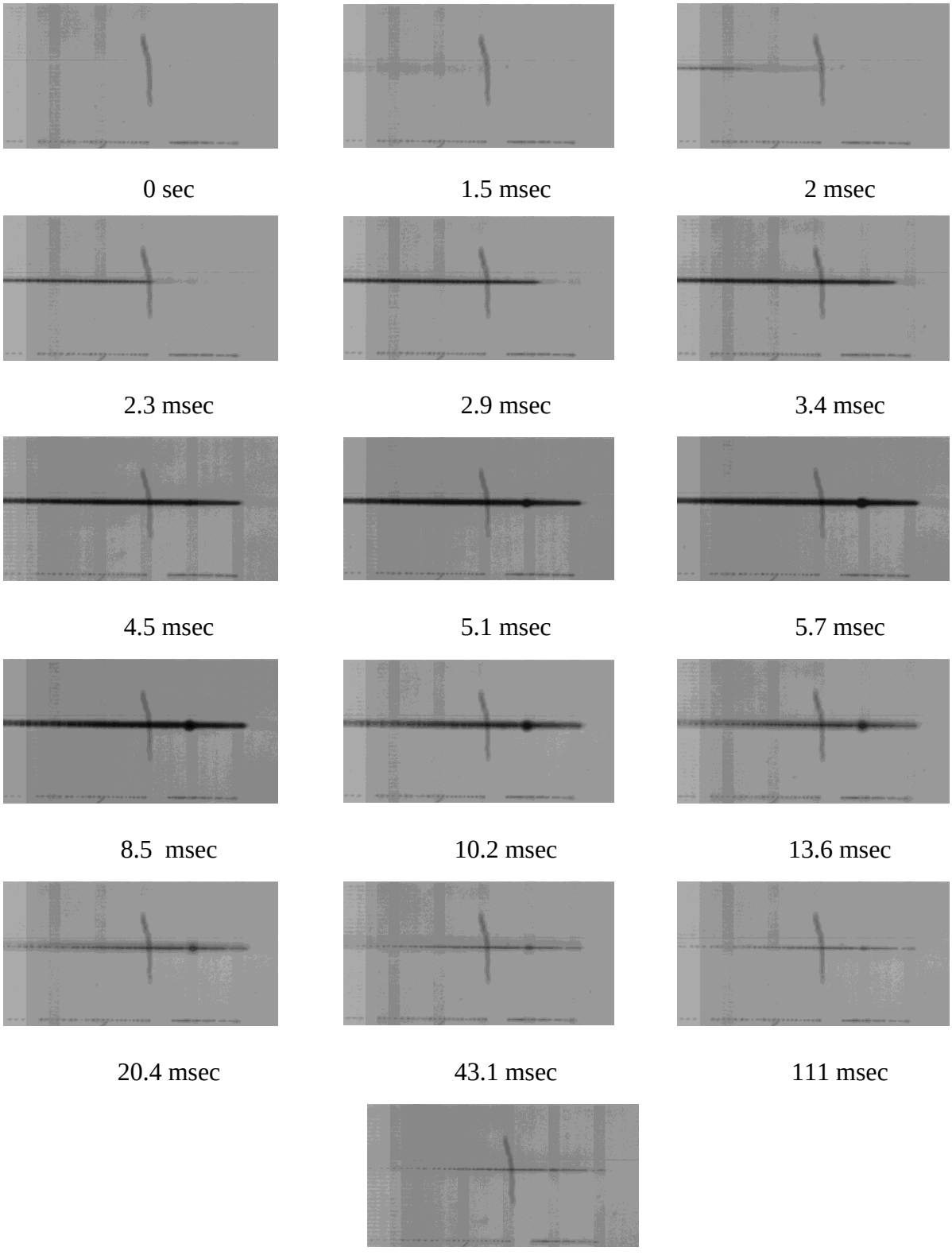

Fig. 20: Phantom High speed camera imaging showing the initiation and growth of the tear in RTV 615 at 5 ms exposure with HIFU operating at 18,300 W/cm^2 captured at 13,029 fps

It is shown in **Fig.20** that the mechanical tear starts at the focal region of the HIFU and starts to grow backwards teaches the maximum size and then grows in size radially. The bubble seen in the images always forms consistently at the same place in the same manner. It is also noted that the time scale of the formation is within the pulse duration while the collapse of the gaps back needs a very long time relative to the time of the gap formation.

In order to understand the mechanism and the mechanical stresses related to the tear formation, LDIC as a technique was utilized in order to measure the deformation in tissue. The experiments to measure and study the effects will be done in the axial and radial sections. **Fig.21 (a)** shows a sample PIV field of an axial section. The HIFU was operated at 5,200 W/cm^2 and a pulse duration of 4316 cycles (1 msec) in order to max sure that the mechanical effect is not in the tearing region found in, and to minimize the thermal effect in order study the mechanical effects alone. **Fig.21 (b)** shows a sample PIV field of a cross-section which shows the deformation in the tissue in the radial direction. The cross-section experiment was operated at 2,500 W/cm^2 and pulse duration of 4316 cycles (1 msec).

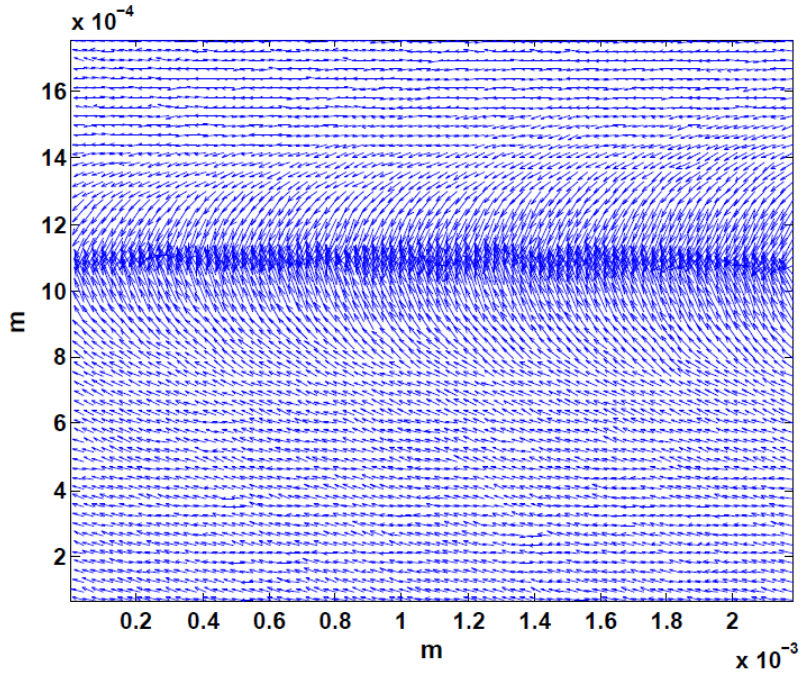

(a)

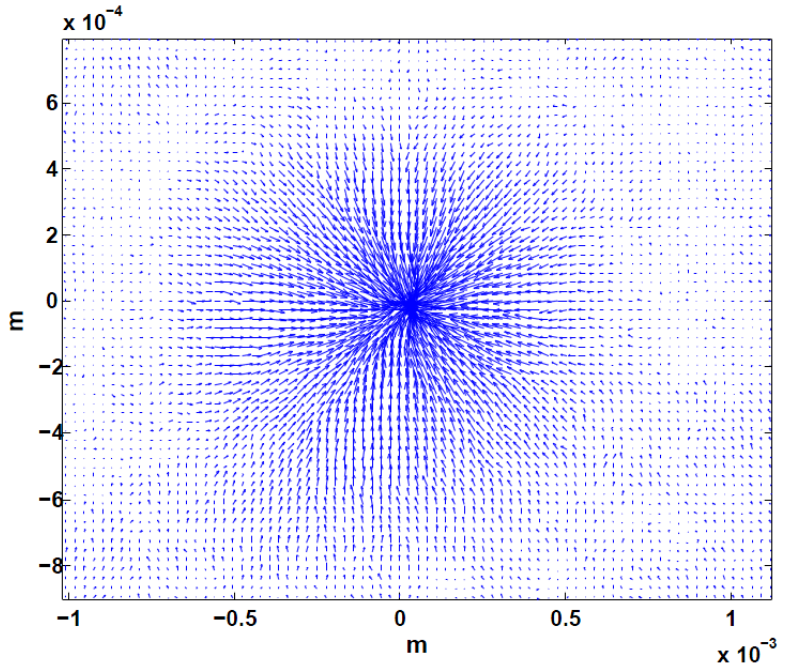

(b)

Fig. 21: (a) axial section of LDIC displacement vector field take at focal intensity of 5,200 W/cm^2 with pulse duration of 1 ms. (b) cross-sectional LDIC displacement field taken at 2,500 W/cm^2 and HIFU pulse duration fo1 ms.

Fig.22 shows the total displacement magnitude $\boldsymbol{D_{total}}$, that is computed by $D_{total} = \sqrt{\Delta x^2 + \Delta y^2}$, of an axial field. The operating powers used in the axial experiment are 2,500 and 5,200 W/cm^2. The HIFU was operated at a pulse width of 4316 cycles (2 msec) in order to reach a large defamation to be able to capture the deformation using the camera CCD. **Fig.23** shows the $\boldsymbol{D_{total}}$ of a cross-sectional field. The HIFU was operated at in the focal intensity rang of 2,500-10,000 W/cm^2. The HIFU exposure was 1079 cycles (0.5 msec) long. The figure shows the effect of increasing the focal intensity on the deformation of tissue after exposure.

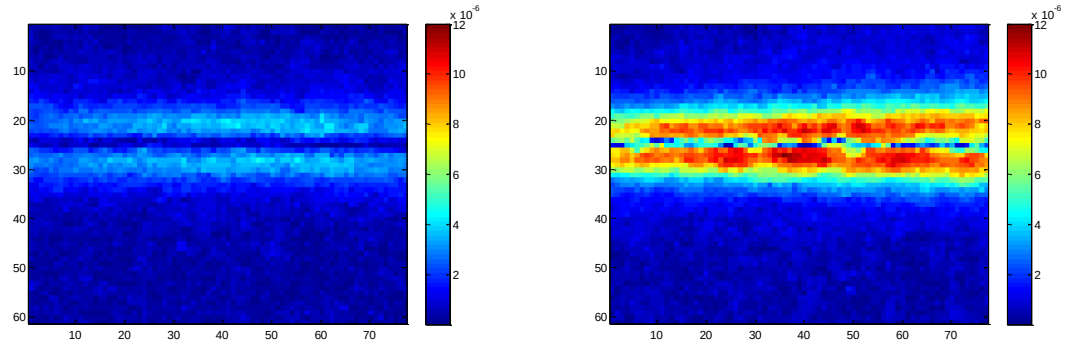

(a) 2,500 W/cm^2 4316 cycles (b) 5,200 W/cm^2 4316 cycles

Fig. 22: $\boldsymbol{D_{total}}$ of an axial displacement field from LDIC in RTV-615 by pulsed HIFU operated at 5,200 W/cm^2 at the end of a 1 msec pulse.

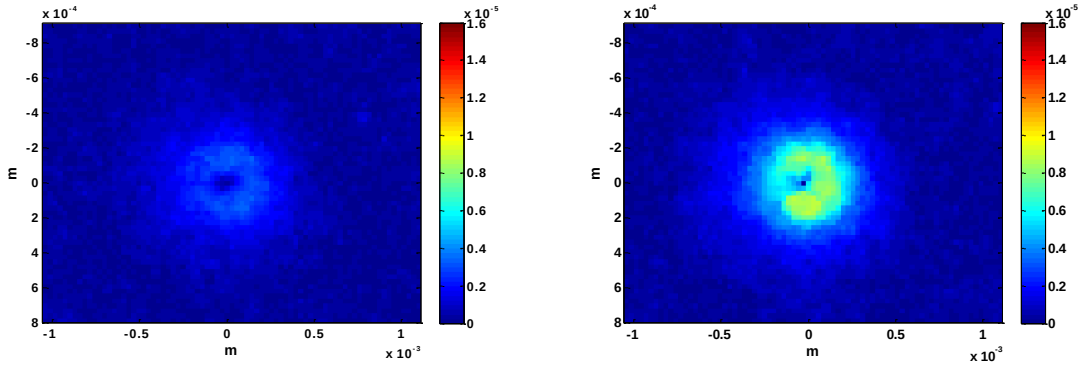

(a) 1079 cycles 2,500 W/cm^2 (b) 1079 cycles 5,200 W/cm^2

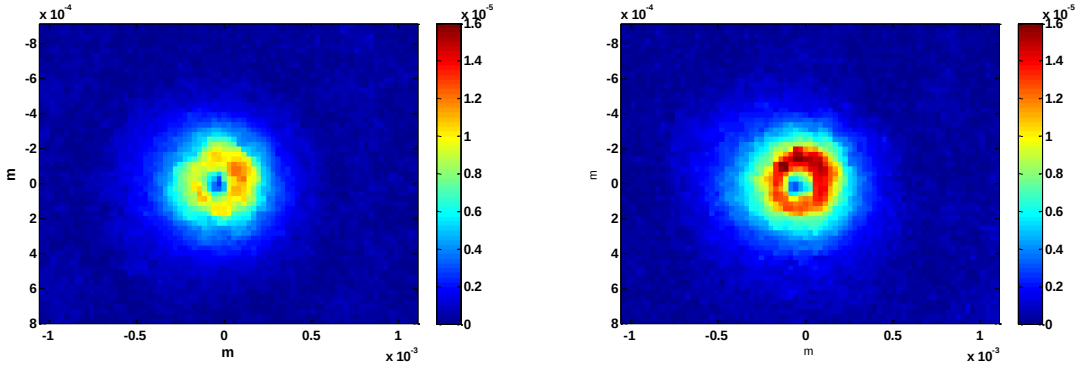

(c) 1079 cycles 7,600 W/cm^2 (d) 1079 cycles 10,000 W/cm^2

Fig. 23: $\boldsymbol{D_{total}}$ of a cross-section displacement field from LDIC in RTV-615 by pulsed HIFU operated at 2,500 W/cm2 at the end of a 1 msec pulse.

Fig.24 shows the cuts of the variation of the deformation of a 0.5 msec burst as the focal intensity increases.

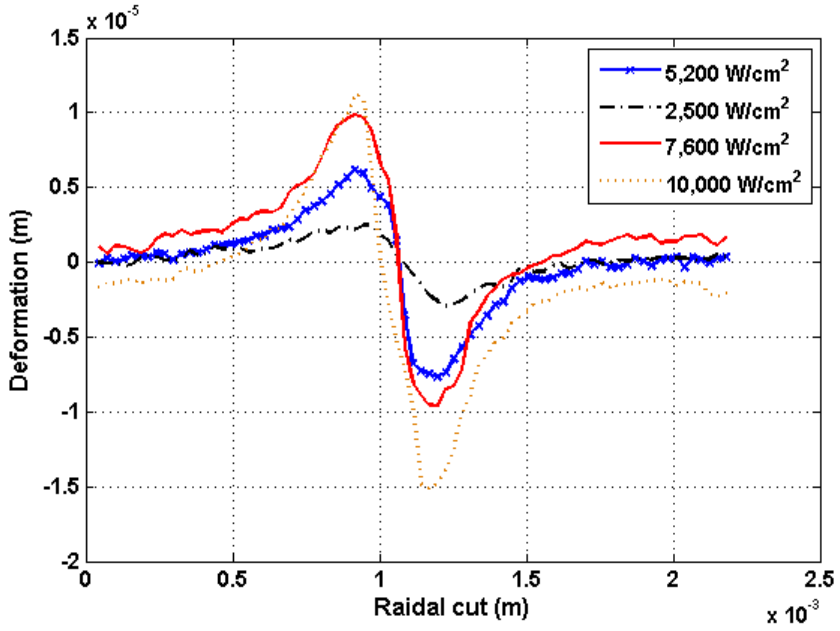

Fig. 24: Cuts through cross-sectinal displacement field determined by LDIC of RTV-615 from pulsed HIFU operated at different focal intensities at 1079 cycles (0.5 msec)

Obtaining the deformation field at the focal point of the HIFU enables the calculation of the strain field inside the tissue. From the strain field there can be a direct measurement of the stress field inside the tissue. In the axial direction the strain fields

(*dU/dx , dV/dy, dV/dx, dU/dy*) were calculated using the least square method, such that *U* and *V* are the horizontal and vertical velocities respectively. However, the magnitudes of all the strain fields were negligible, except the *dV/dy* field. The strain fields leads to a conclusion that the mechanical effects at the focal point are pure compression in the radial direction as the vector fields and strain fields indicate. **Fig.25** shows the strain field (*dV/dy)* in the axial focal point section experiment, the HIFU was operated at focal intensity of 5,200 W/cm^2 at a burst length of 4316 cycles (2 msec). Calculating the stress field in **Fig.26** by the strain field is simply achieved by multiplying the strain field by the modulus (***1.91 MPa***) of elasticity provided by the material manufacturer (RTV-615, GE, USA). The maximum stress measured at the location were tearing initiates were measured to be in the order of *0.12 MPa* at 2,500 W/cm^2 and *0.4 MPa* at 5,200 W/cm^2.

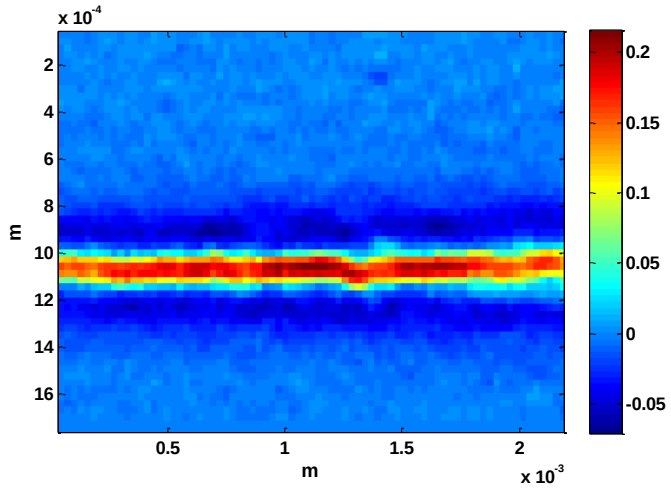

Fig. 25: *dV/dy* Strain field determined using least square method using deformation field aquired by LDIC experiment of pulsed HIFU operated at focal intensity of 5,200 W/cm^2 and pulse duration of 4316 cycles

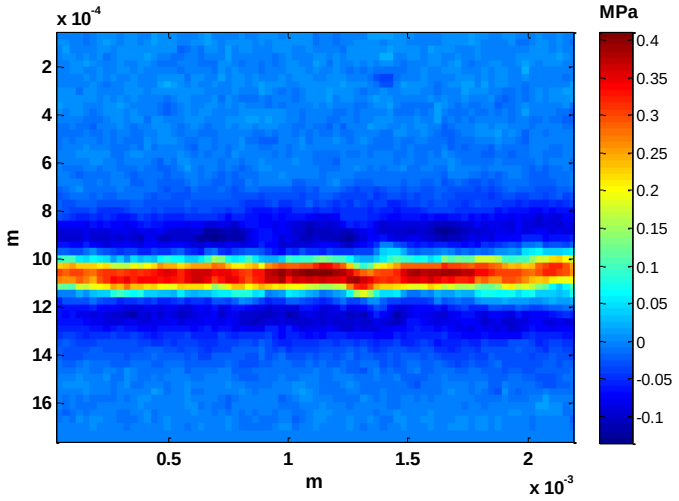

Fig. 26: Axial stress field of a pulsed HIFU at focal intensity of 5,200 W/cm^2 and a pulse duration of 1 msec

3.4. High Intensity Focused Ultrasound Transducer Calibration:

The experiment was performed in the range of voltages between **Fig.27** the change in mass measured (mg) by the analytical balance at fundamental voltages between 33.67, 67, and 96.9 V_{pp}. The data from the analytical balance was processed to calculate the Force (N) that is transmitted by the transducer lifting the absorber rubber. To make sure there are no streaming effects on the absorber rubber leading to over estimation or bias of the results, an experiment with a thin saran wrap film was placed directly before the target limiting any acoustic streaming activity in water towards the target. **Fig.28** shows the two experiments performed with and without saran wrap film. The result of the RFB force on the target shows that the effects of the acoustic streaming is minimal due to the very low distance between the target and the HIFU face which is maintained less than 2 cm in all experiments which is less than half the distance to the focal point (4.4 cm).

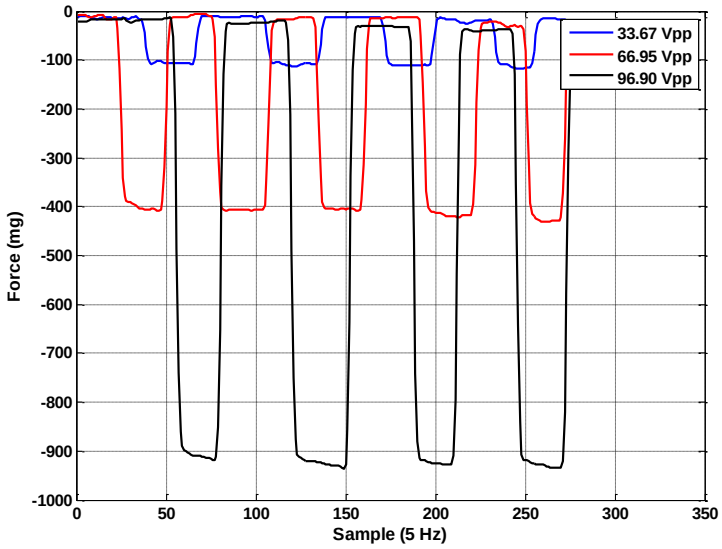

Fig. 27: Radiation force balance setup force on acoustic absorber.

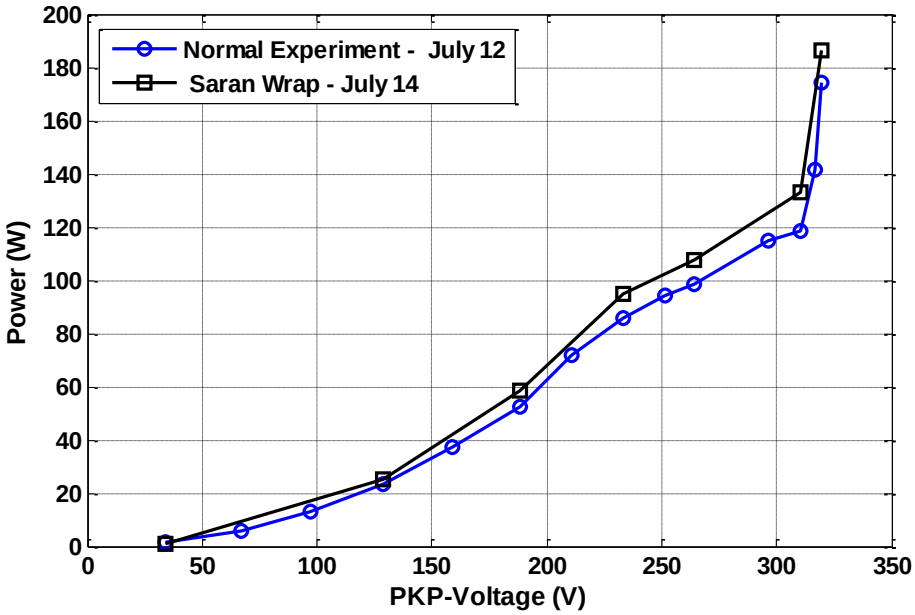

Fig. 28: Radiation force balance experiment calibration curve of the acoustic power vs. the peak to peak voltage input to the transducer with and without saran wrap to avoid streaming

The biased points due to heating of the absorber target that is pronoun in the operating fundamental voltages above 300 Vpp, are corrected for by fitting the linear unbiased point and extrapolating the biased points using the fitted linear function. The linear relation between the acoustic power and the operating electric power is used to

determine the extrapolation of the points in the study to calculate the focal intensities. The outlier points that are of the operating voltages above 300 Vpp are taken out from the curve. The efficiency of the transducer is calculated to be 68.2%. The rest of the curve is extrapolated using the calculated efficiency. The corrected HIFU transducer calibration is shown is **Fig.29**. The focal intensity is calculated by dividing the measured acoustic power over the -6db area measured by a hydrophone to be 0.1 mm in diameter.

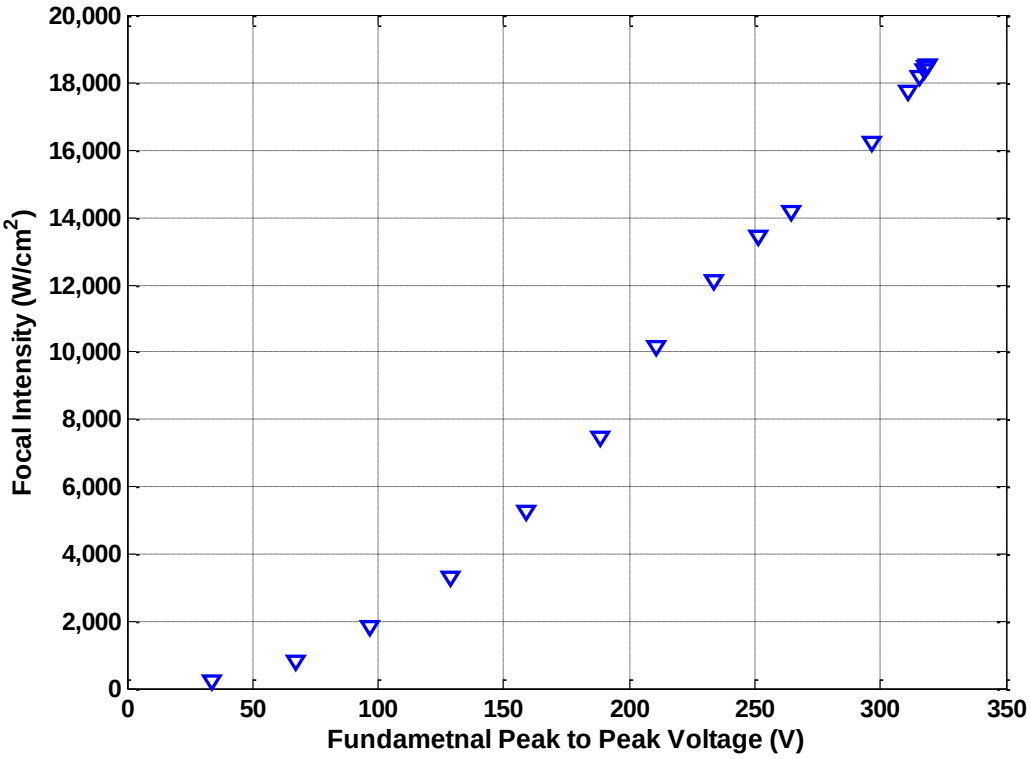

Fig. 29: The Fundamental peak to peak voltage vs. The focal intensity of the HIFU transducer determined by the RFB setup

CHAPTER 4

DISCUSSION

Motivated by a desire to resolve the fast heating rates and mechanical effects from pulsed HIFU exposure at pressure levels associated with non-linear US propagation and focal shock formations in water in the case of heating, we have set out to demonstrate a non-invasive LIF thermometric tool capable of capturing the fast heating in the focal region in free field water. The technique is based on calibrating the temperature dependent fluorescence light emissions from an aqueous dye solution present in the focal region.

We utilized a replica of the HIFU transducer characterized by Canney et al. (2008) and found to produce shock waves in the focal region at intensities above 6,000 W/cm2; and later found by Canney et al. (2010) to cause millisecond boiling in gels (heating rates from 2,000 to 20,000). An increase of 50-83 times in the absorption of gels has been reported due to shock-induced heating. Our transducer was operated at input power levels producing focal intensities between 5,200 to 18,500 W/cm2, i.e., the range for which shocks form.We made use of the available PIV technique to demonstrate the non-linear propagation characteristics of the US waveform in the focal region. Specifically, we measured the waveform of the acoustic particle velocity in the focal region at a high power causing heating (18,500 W/cm2) and at a low power that produced no detectable heating (1,200 W/cm2). The two acoustic velocity waveforms are presented in **Fig.30 (a)**. The timing between the two PIV exposures was set to, which was short enough to capture a single US wave, but too long to capture the instantaneous particle velocity. So the measured velocity was effectively averaged over nearly half a wave period. Comparable acoustic velocity magnitudes were measured by

Haller et al. (2011) in a HIFU field. The figure demonstrates the linear wave propagation in the non-heating case, and the non-linear wave propagation as seen from the deformed shape of the waveform in the heating case (in 3 ms). The phase shift is likely due to the averaging artifact mentioned earlier. The two dimensional velocity vector fields for the non-heating (linear propagation) and the heating (non-linear propagation) cases are shown in **Fig.30 (b)** and **30 (c)**, respectively. Thus non-linear wave propagation in the focal volume and the higher harmonics (in addition to the fundamental frequency) are the source of the free field heating. One should lastly emphasize that due to the time averaging over nearly 1/2 the wave period, comparison of the peak velocities is not justified. It is the non-linear waveform shape at high intensities that is intended in this figure.

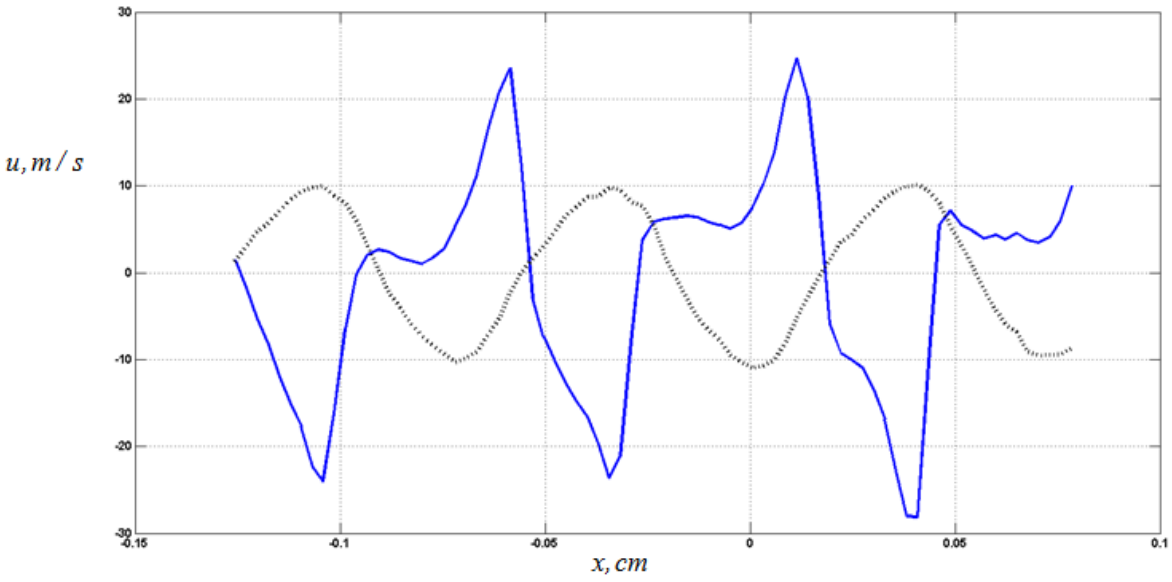

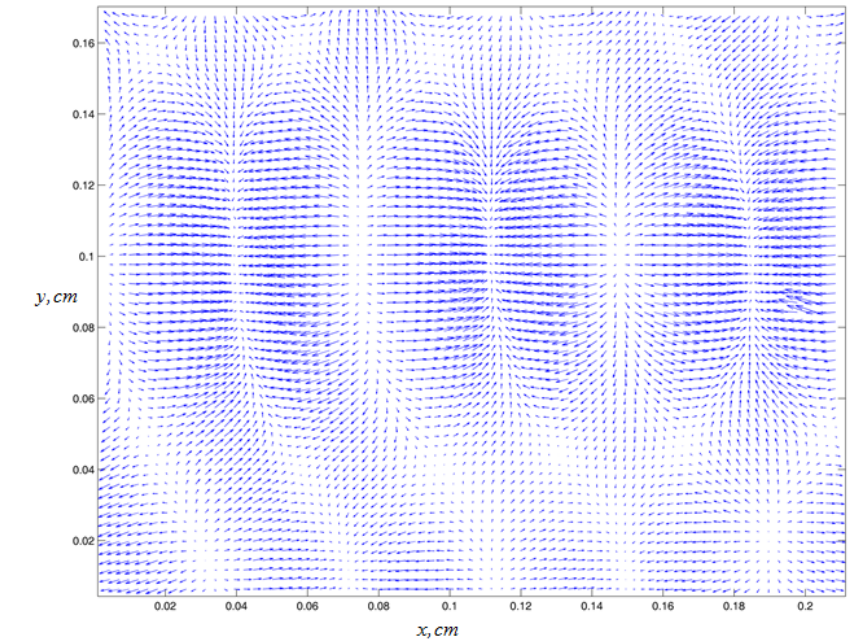

(b)

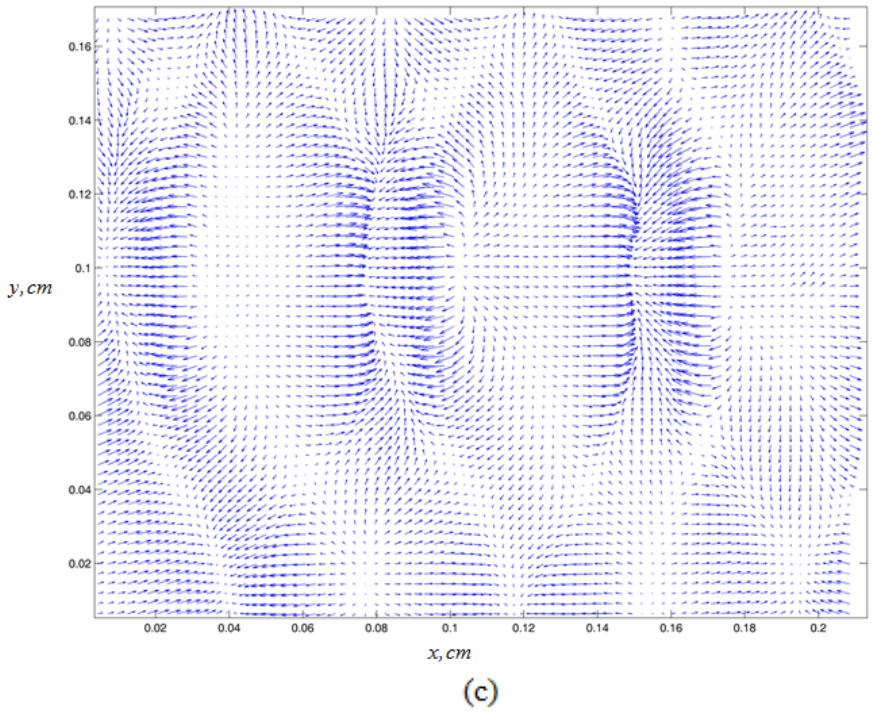

(c)

Fig. 30: (a) Acoustic particle velocity waveform in the HIFU focal region measured with PIV. The two PIV image exposures are taken 250 ns apart at the end of a 15-cycle burst. Each curve is averaged from 40 instantaneous vector fields. (b) the 1200 W/cm2 focal intensity; and (c), the 18,500 W/cm2 focal intensity. The US propagation is from right to left.

However, looking at **Fig.31** shows that taking the total velocity $\boldsymbol{V_{total}}$ calculated by $\boldsymbol{V_{total}} = \sqrt{\boldsymbol{U^2 + V^2}}$, such that U and V are the horizontal and vertical velocities respectively. That as the focal intensity is increase the wave rather gets thinner and steeper than phase shit. The wave form shows evidence of shock formation in the range at which heating is detectable (at focal intensities of 5,200 W/cm^2 and above). At the focal intensity of 1,200 W/cm^2 the wave form shows more or less a linear propagation were no distortion to the sine wave form is observed.

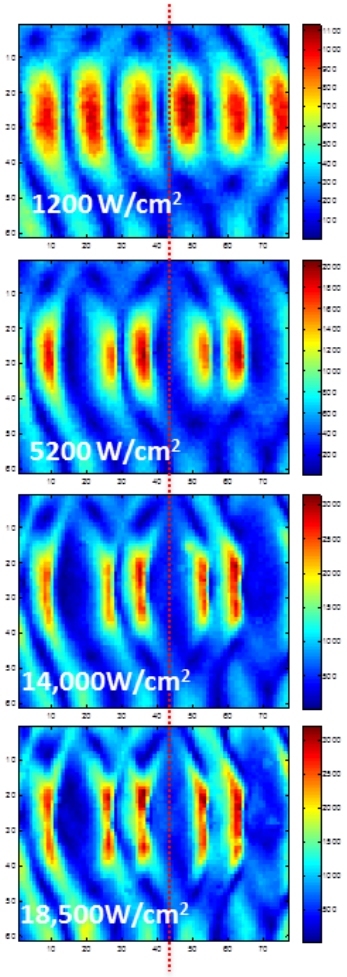

Fig. 31:(a) total acoustic particle velocity field in the HIFU focal region measured with PIV at the end of a 15-cycle burst at different focal intensities showing the narrowing of the waves that caused the phase shift in the cuts.

We have been able to measure the fast (better than 50 ns rise time) temperature rise in water with sub millimeter resolution. The maximum attained temperature rise was 4 °C (at 18,500 W/cm2 focal intensity). The heating rate measured to be at the range of 4,000 to 7,000 ^{0}C/sec. This is in general agreement with the heating rates (1,600 ~ 20,000 ^{0}C/sec) found with shock-enhanced heating and millisecond tissue boiling by Canney et al. (2010). Without considering the effect of non-linear propagation from shock formation on heating, it would indeed be quite a surprising result that the heating rates in the highly absorptive gel and in the nearly lossless water are comparable, as one would expect much higher heating rates in the gel. However, due to shock formation, the absorption in water is expected to increase due to the presence of the higher harmonics. The following equation shows a simplified formula in which the heating rate is calculated depending on linear wave propagation.

$$\frac{\partial T}{\partial t} = \frac{I e^{-2\alpha L}}{\rho C_p L}$$

Where α is the acoustic absorption of water, L in the length of the focal spot at which the shock is forming, C_p is the specific heat of water, ρ is the water density. If we assume the properties of water at the focal point to have an acoustic absorption of 0.9314 db/m, a density of 1000 kg/m^3, and the specific heat to be 4.181 kJ/kg.K, and assuming a focal spot with the length of 0.2 mm (two diameters). The heating rate would be calculated to be 22 deg C/ sec. This value is 316 times less than the value measured experimentally. However there are several points to be taken into consideration, the narrowing of the focal spot in the axial and transvers directions, the increase in the acoustic absorption due to shock-formation. The focal spot length in the paper by Bessonova et al (2009), shows narrowing of the focal spot from ~ 0.2 mm to as

small as ~ 0.02 mm. applying this reduction of our assumed value without any change in the acoustic absorption shows an increase in the heating rate (221 deg C/sec), which is only 31 times less than the experimentally measured heating rate.

Moreover, shock pressures in water are expected to be significantly higher than in gel due to the negligible path losses. As the length of the HIFU burst was increased beyond 3 ms, the water heating rate at the focus dropped to nearly zero. PIV was used to measure the instantaneous streaming velocities around the focal point to assess the role of convective cooling on the drop in the heating rate. The PIV data demonstrated that the streaming velocity was minimal for short bursts (2 cm/sec for a 0.125 ms burst) when the focal heating rate was 7000 ^{0}C/sec. Mean convective streaming developed and intensified with increasing length of burst, and the convective cooling effect also strengthened. For example, for a 2 ms burst the mean streaming velocity in the focal spot region was 0.6 m/sec, while the rate of temperature rise dropped significantly from the peak levels stated above. The heating rate became nearly zero for bursts 3 ms or longer, when the measured streaming exceeded 1 m/s. For it to be of significance at reducing the water temperature rise, streaming has to generate velocities on the order of (1 m/s) in the focal region. At this velocity level and at the time scale of interest (1 ms), the convective mass transfer rate becomes sufficient to cause a turnover of the heated focal volume fluid (1 mm), and to replace it with a fresh volume of cool ambient fluid. It was noted also that the streaming flow at the focus caused a deviation in the transverse cross sectional shape of the heated spot from axis-symmetry likely due to the formation of flow instabilities as suggested by the PIV findings of Hariharan et al. (2008).

The use of laser fluorescence imaging allowed the visualization of the spherical sound focusing which provided an accurate spatial reference of the focus location. More importantly, an optical thermal lensing shadow was seen in the images. It was caused by alterations in the water's optical refractive index from the localized HIFU heating.

Lastly, it would be of significant interest and relevance to extend the LIF technique from a water medium to the study of gels and tissue mimicking phantoms. The basic requirement in such an extension is the optical transparency of the medium to allow for deep field imaging. We have applied LIF to an agar-based gel phantom using the same methodology described earlier, and we were able to detect heating from ms sound pulses clearly. However, the increased presence of scatterers in the grainy agar gel added a layer of uncertainty to the temperature measurements. By using a different, optically clear phantom material (moldable RTV rubber, supplied as liquids A+B) we noticed that after the mold had solidified, the Rhodamine dye fluorescence lost its thermal sensitivity. It is possible that using a different fluorescence dye such as fluorescein may produce a more positive outcome. We also speculate that using a water-based clear gel material would extend the applicability and reliability of LIF for thermometry in soft solids.

In the other hand, in the objective of studying the initiation of tears/gaps inside tissue mimicking phantoms, and the mechanical effects upon the interaction of HIFU with tissue, RTV-615 as a tissue mimicking material was used. RTV-615 as a tissue mimicking material reported by (Maggie, 2011), as being very similar to human tissue properties in terms of ultrasound propagation and mechanical and thermal properties. The RTV-615 was held in strong vacuum before and after mixing to insure no degasification of any dissolved bubbles in the tissue mimicking material during

insonification. Permanent damage was observed in tissue within milliseconds of exposure. The damage can be caused by mechanical effect due to the stresses associated with the wave pressure shockwaves and radiation force. However, thermal effects can have a major role especially when shockwave heating is present. It has been reported that mechanically formed gaps can be caused by pulsed HIFU (Hancock et al., 2009). However, the mechanism behind this gap formation is still unclear. It has been speculated that the gaps are formed due to mechanical stresses; models using FEM have pushed aiding the theory behind their formation mechanically. Thermal effect within the region of tears in our experiment has a role but it is mostly not considered to be a major role. The mechanical stresses are thought to be the driving force behind the formation of the tears/gaps. In **Fig.19** it shows that the tears in tissue, are related not only to the focal intensity at which they occur, rather they are a result of a time averaged event that evolve with the focal intensity, pulsed exposure duration. However, for each HIFU focal intensity a length of tear threshold exists that cannot be exceeded. This indicated that it has a direct relation with the pressure distribution at the focal region, rather than a thermal region that should be growing with increasing the pulse exposure duration.

Fig.20 shows that the tear starts at the focal point and start to grow backward post focally while increasing the length of burst and stops at a certain point depending on the focal intensity. The shape and form of the gap is consistent from pulse to pulse in shape and length at a certain focal intensity. The time scale at which the tear occurs is within the HIFU pulse width. However, the time associated with the collapse of the gap formed takes than 20 times the time of formation. After the collapse of the gap, a permanent damage can be still seen inside the tissue as shown in **Fig.18**.

In order to study the mechanical effect due to the pulsed HIFU the thermal effects due to HIFU must be minimized and damage to the tissue mimicking material should be avoided. Thus, focal intensities below 5,200 W/cm^2 and pulse durations below 4316 cycles (2 msec) were used in our study. Nano particles were added to RTV-615, to enable the use of LDIC technique, to visualize the deformation field in the cross-section and axial section of the HIFU focal point. It is expected to observe micro scale deformation as reported (Hancock et al. 2009; Myers 2006). It is common in literature that the radiation force due to pulsed HIFU cases pushing of the material. The theory would make sense if the force at the tear region is causing the tears to form. However, The direction of the mechanical strain in the focal region is visualized and quantified to be pure compression. Thus, the formation of the gap can be due to the compressive stress caused by the shockwaves passing through the focal point that leads to failure of the material. The consistency of the shape and size of the tear is due to the homogeneity of RTV-615.

The study of the causes and mechanism behind the formation of gaps, and the mechanical stresses associated with pulsed HIFU in tissue can be of relevance to the use of HIFU in drug delivery and harmonic motion imaging (HMI) for tumor diagnostic and treatment. The understand of the mechanical stresses and strain in tissue can be of huge relevance to those fields. The gap formation in tissue can also have significantly important role in drug delivery, as discussed before it is speculated that it is a major player in the opening of the blood brain barrier to chemotherapy. However, this won't be possible without quantifying the mechanical and thermal effects non-invasively inside tissue due to pulsed HIFU. This would lead to the understanding of the role of the thermal and mechanical output in tissue in the formation of tears. We were able to

measure the mechanical strain in tissue to be as high as 0.2 at the focal point in tissue at 5,200 W/cm^2 after 4316 cycles. The measured strain field gives a direct evidence of a mechanical mechanism at the focal region due to the interaction with the focused ultrasound waves that has a major role in the formation of the tear/gap. Nevertheless, more investigation needed to insure the role of the mechanical stresses in the formation of the gap and the nature of it as a burn or mechanical failure in the tissue.

CHAPTER 5

CONCLUSION

A laser-induced fluorescence thermometry technique for the measurement of localized heat deposition in water from shocking HIFUs was demonstrated experimentally. It provided good spatial and temporal resolutions to quantify millisecond heating in water. Non-linear wave propagation from shocking in the focus was believed to be the cause of enhanced heating and increased ultrasound absorption in water where a temperature rise of 4 °C was detected. The water temperature rise increased with increasing focal power intensity. A heating rate of 7000 °C/sec was observed. This fast heating was consistent with the shock-enhanced boiling in gels found by Canney et al. (2010). Mean acoustic streaming was measured and found to induce a dominant cooling effect in water within only 2~3 ms from the onset of the sound burst and thus placing an upper limit on the temperature rise. Permanent damage to tissue mimicking material RTV-615 was observed due to pulsed HIFU. Furthermore, the mechanical effects of pulsed HIFU were investigated in tissue mimicking materials as a mechanism causing tears. The mechanical deformation due to wave propagation emitted by a HIFU source was visualized using Laser Digital Image Correlation method in RTV-615, and was found to be 16 μm, and a strain of 0.2.

REFERENCES

Vivies, A. A., Arnau, A., Soares. D., Fundamentals of Piezoelectricity, Piezoelectric Transducers and Applications, Springer-Verlag Berlin Heidelberg 2008, doi: 10.1007/978-3-540-77508-9_1.

Bailey M. R., Khokhlova V. A., Sapozhnikov O. A., Kargl S. G., and Crum L. A. Physical Mechanisms of the Therapeutic Effect of Ultrasound (A Review). Acoustical Physics 2003; Vol. 49(4), pp. 369–388

Banerjee, R.K., Dasgupta, S. Characterization Methods of High-Intensity Focused Ultrasound-Induced Thermal Field," Advances in Heat Transfer 2010; 42 (C), pp. 137-177; ISSN: 00652717

Bessonova O.V., Khokhlova V.A., Bailey M.R., Canney M.S., Crum L.A., Focusing of High Power Ultrasound Beams and Limiting Values of Shock Wave Parameter, Acoust Phys. 2009; Vol. 55(4-5), pp 463–476

Brujan EA, Ikeda T, Yoshinaka K, Matsumoto Y. The final stage of the collapse of a cloud of bubbles close to a rigid boundary," Ultrasonics Sonochem. 2011; Vol 18, pp59-64

Cheng, Y., Li, R., Li, S., Dunsby, C., Eckersley, R. J., Elson, D. S., Tang, M., 2012; Ultrasound in Med. & Biol., Vol. 38, No. 9, pp

Canney M.S., Bailey M.R., Crum L.A., Khokhlova V.A., and Sapozhnikov O.A. Acoustic characterization of high intensity focused ultrasound fields: A combined measurement and modeling approach. J. Acoust. Soc. Am. 2008; Vol. 124, Issue 4, pp. 2406-2420

Canney MS., Kholkhova VA, Bessonova OV., Bailey MR, and Crum LA. Shock-induced heating and millisecond boiling in gels and tissue due to high intensity focused ultrasound. Ultrasound in Med. & Biol. 2010; Vol. 36(2), pp. 250–267

Chen, D., Fan, T., Zhang, D., and Wu, J. A feasibility study of temperature rise measurement in a tissue phantom as an alternative way for characterization of the therapeutic high intensity focused ultrasonic field. Ultrasonics 2009; 49(8), 733–742

Chitnis PV, McLaughlan J, Mamou J, Murray T and Roy RA. A photoacoustic sensor for monitoring in situ temperature during HIFU exposures. 9th Int. Symp. Therapeutic Ultrasound ISTU 2009; pp 267-272

Clark R.L., and ter Haar G.R. Temperature rise recorded during lesion formation by high-intensity focused ultrasound. Ultrasound Med. Biol. 1997; 23 (1997) 299–306

Crimaldi JP. Planar laser induced fluorescence in aqueous flows. Exp. Fluids 2008; Vol 44(6), pp 851-863.

Curra, F.P. and Crum, L.A. Therapeutic ultrasound: surgery and drug delivery. Acoust. Sci. Technol. 2003; 24(6), pp 343–348.

Dasgupta S., Wansapura J., Hariharan P., Pratt R., Witte D., Myers M. R., and Banerjee R. K. HIFU lesion volume as a function of sonication time, as determined by MRI, histology, and computations. J. Biomech. Eng. 2010, 132(8).

Danehy PM, and Alderfer DW. Survey of temperature measurement techniques tor studying underwater shock waves. Int. Symp. on Interdisciplinary Shock Wave Research 2004; Sendai Japan, 22-24 March, 2004

Farny, C.H., Holt, R.G., Roy, R.A. Temporal and Spatial Detection of HIFU-Induced Inertial and Hot-Vapor Cavitation with a Diagnostic Ultrasound System. Ultrasound in Med. & Biol. 2009; 35 (4) , pp. 603-615

Hancock, A. H., Smith, L. H., Cuesta, J., Durrani, A. K., Anfstadt, M., Palmeri, M. L., Investigation in Pulsed HIFU-Enhanced Delivery: Preliminary Evidence of Novel Mechanism. Ultrasound in Med. & Biol., 2009; Vol. 35, No. 10, pp. 1722–1736,

Hall L. On the origin of ultrasonic absorption in water. Phyiscal Rev. 1948,Vol 73(7), pp 775-781

Haller J, Wilkens V, Jenderka K-V, and Koch C. Characterization of a fiber-optic displacement sensor for measurements in high-intensity focused ultrasound fields. J. Acoust. Soc. Amer. 2011; Vol 129(6), pp 3676-3681.

Hallez L., Touyeras F., Hihn JY, and Klima J. Energetic balance in an ultrasonic reactor using focused or flat high frequency transducers. Ultrasonics 2007; 14, 739–749.

Han, D., and Mungal, M. G. Simultaneous Measurements of Velocity and CH Distributions. Part 1: Jet Flames in Co-Flow. Combust. Flame 2003; Vol. 132, pp. 565–590.

Hariharan P, Myers MR, Robinson RA, Maruvada SH, Sliwa J, and Banerjee RK. Characterization of high intensity focused ultrasound transducers using acoustic streaming. J. Acoust. Soc. Am. 2008; Vol 123(3), pp 1706-1719

Harris GR. Progress in medical ultrasound exposimetry. IEEE Ultrasonics, Ferr., Freq. Control 2005; Vol 52(5), pp 717-736

Holbrook AB, Santos JM, Kaye E, Rieke V, Butts Pauly K. Real-time MR thermometry for monitoring HIFU ablations of the liver. Magn Reson Med 2010; Vol 63:365–373

Huang, J., Holt, R. G., Cleveland, R. O., and Roy, R. A. Experimental validation of a tractable numerical model for focused ultrasound heating in flow-through tissue phantoms. J. Acoust. Soc. Am. 2004; Vol 116, 2451–2458

Jolesz FA. MRI-guided focused ultrasound surgery. Annual Rev. Medicine 2009, Vol. 60, pp.417-430

Kyuichi, Y., Fundamentals of Acoustic Cavitation and Sonochemistry, Theo. and Exp. Sonochemistry Involving Inorganic Sys., Springer, 2011; pp 1-29

2010, pp 1-29

Kaiser A, Cain C, Hwang E, Fowlkes J, and Jeffers R. A cost effective degassing system for use in ultrasonic measurements: The multiple pinhole degassing system. J. Acoust. Soc. Am. 1995; Vol. 99, pp. 3857–3860

Khokhlova, V.A., Bailey, M.R., Reed, J.A., Cunitz, B.W., and Kaczkowski, P.J. Effects of nonlinear propagation, cavitation, and boiling in lesion formation by high intensity focused ultrasound in a gel phantom. J. Acoust. Soc. Am. 2006; 119(3), pp. 1834–1848.

Khokhlova, T.D., Canney, M.S., Lee, D., Marro, K.I., Crum, L.A., Khokhlova, V.A., Bailey, M.R. Magnetic resonance imaging of boiling induced by high intensity focused ultrasound," J. Acoustical Soc. of Am. 2009; Vol. 125 (4), pp. 2420-2431

Lighthill, J. (1978). Acoustic streaming." Journal of Sound and Vibration 61(3): 391-418

McLaughlan J, Rivens I, Leighton T, and ter Haar G. A Study of Bubble Activity Generated in Ex Vivo Tissue by High Intensity Focused Ultrasound. Ultrasound Med. Biol. 2010, Vol. 36(8), pp 1327–1344

Morris, H., Rivens, I., Shaw, A., and ter Haar, G. Investigation of the viscous heating artifact arising from the use of thermocouples in a focused ultrasound field. Phys. Med. Biol. 2008; Vol. 53, 4759

Maggi, L.E. , Development of silicon-based materials for ultrasound biological phantoms, Ultrasonics Symposium (IUS), 2009 IEEE, pp 1962- 1965

Neppiras, E. A., Acoustic Cavitation, 1st Edition, North-Holland Publishing Company, 1980, Amsterdam, Vol.3, pp 159—251.

Nightingale, K., Soo, S. M., Nightingale, R., Trahey, G., Acoustic Radiation Force Impulse Imaging: In Vivo Demonstration of Clinical Feasibility, Ultrasound in Med. & Biol., 2002; Vol. 28, No. 2, pp. 227–235

Nishihara, T., Utashiro, H., Ichiyanagi, M., Yoshinaka, K., Takagi, S., Matsumoto, Y. Heating location control of HIFU treatment enhanced with microbubbles. AIP Conference Proceedings 2011; 1359, pp. 235-240

Qian, Z. W., Xiong, L., Yu, J., Shao, D., Zhu, H., and Wu, X. Non-invasive thermometer for HIFU and its scaling. Ultrasonics 2006; Vol. 44, pp: e31–e35.

Rossing, T. D., Physical Acoustics In. Springer Handbook of Acoustics; 1st Edition, Springer: New York, 2007; pp 207-238.

Rossing, T. D., Non-Linear Acoustics In. Springer Handbook of Acoustics; 1st Edition, Springer: New York, 2007; pp 257-297.

Raffel M, Willert CE, Kompenhans J. Particle Image Velocimetry: A Practical Guide. 1998, Springer-Verlag.

Seip, R., Ebbini, E.S. Noninvasive estimation of tissue temperature response to heating fields using diagnostic ultrasound. IEEE Transactions on Biomedical Engineering 1995; Vol. 42 (8), pp. 828-839

Seuntiëns HJ, Kieft RN, Rindt CCM, and van Steenhoven AA. 2D temperature measurements in the wake of a heated cylinder using LIF. Exp. in Fluids 2001; Vol. 31, pp 588-595

Shaw A, Hodnett. Calibration and measurement issues for therapeutic ultrasound. Ultrasonics 2008, Vol. 48(4), pp 234–252

Shaw A, Khokhlova V, Bobkova S, Gavrilov L, and Hand J. Calibration of HIFU intensity fields measured using an infra-red camera. Advanced Metrology for Ultrasound in Medicine (AMUM 2010) Journal of Physics 2011: Conference Series 279

Song, C., Marshall, B., McLean, D., Frank, T., Cuschieri, A., Campbell, P., and Sibbet, W. Thermo graphic investigation of the heating effect of high intensity focused ultrasound. Conf. Proc. IEEE. Eng. Med. Biol. Soc. 4 2005; pp. 3456–3458

Speyer, G., Kaczkowski, P.J., Brayman, A.A., Crum, L.A. Displacement analysis of diagnostic ultrasound backscatter: A methodology for characterizing, modeling, and monitoring high intensity focused ultrasound therapy. J. Acoustical Soc. of Am. 2010; Vol. 128 (1), pp. 104-120

Sutton JA, Fisher BT, Fleming JW. A laser-induced fluorescence measurement for aqueous fluid flows with improved temperature sensitivity. Exp. Fluids 2008; Vol. 45, pp 869-881

ter Haar G. Therapeutic applications of ultrasound. Progress in Biophysics and Molecular Biology 2007; Vol. 93, pp 111–129

Vogel A., and Noack J. Shock wave energy and acoustic energy dissipation after laser-induced breakdown. SPIE Proc. 1998; Vol. 3254, pp. 180-189.

Winkel, E. S., Oweis, G. F., Vanapalli, S. A., Dowling, D. R., Perlin, M., Solomon, M. J., Ceccio, S. L. High-Reynolds-number turbulent boundary layer friction drag reduction from wall-injected polymer solutions. J. Fluid Mech. 2009; Vol. 621, pp. 259-288